Preliminary Evidence of Transport-Limited Chemical Weathering and Element Immobility in the Ganges Tidal Delta Plain of Bangladesh

J. C. Ayers[1], B. Patton[1], and M. Dietrich[1]

[1] Department of Earth and Environmental Sciences, Vanderbilt University. VU Station B, #351805, 2301 Vanderbilt Place, Nashville, Tennessee 37235-1805, U. S. A.

Corresponding author: John C. Ayers (john.c.ayers@vanderbilt.edu)

Key Points:

- In the Ganges tidal delta plain in Bangladesh chemical weathering rates are low and transport-limited.
- Tidal channel sediments and rice paddy soils are similar in composition to average upper continental crust.
- Relative to coexisting solids surface waters are depleted in immobile elements but are not in exchange equilibrium.

Abstract

Previous studies have documented a weathering-limited regime in the upper reaches of the Ganges River Basin. Chemical weathering and element mobility in the lower reaches of the Ganges in the tidal floodplain of Southwest Bangladesh were investigated by comparing compositions of rice paddy soils, precursor tidal channel sediments, surface waters, and extract solutions, which represent the soluble fraction of solids. Little spatial variation in water and solid compositions is observed in each season, indicating similar processes are acting to transport elements across this region. Roughly one to several decades after deposition, rice paddy soils are not significantly different in mineralogy or composition from precursor tidal channel sediments, and both are similar to the composition of average upper continental crust. There is no detectable change in composition of tidal channel water between upstream and downstream sites. Rice paddy and tidal channel waters are saturated in the dominant minerals present in the silt-sized soils and sediments, which are dominantly quartz and clay minerals. Together, these observations indicate the dominance of weathered material and low chemical weathering rates in the tidal floodplain, consistent with a transport-limited regime. Multiple lines of evidence indicate a lack of exchange equilibrium between surface waters and coexisting solids, which may be a common feature in tidal river deltas where transport-limited regimes likely dominate.

Plain Language Summary

Previous studies of the upper reaches of the Ganges River near the Himalaya have shown that an abundant supply of easily weathered minerals produced by erosion results in rapid weathering and transport of large amounts of dissolved material in the river. We measured the chemical compositions of water from rivers and rice paddies, and of associated river sediments and the soils that form from them, in the lower reaches of the Ganges River tidal delta plain in SW Bangladesh. We found that soils were similar in composition to river sediments, and that river water compositions were constant across our study area. These observations suggest that little material is transferred from solids to water over the course of roughly one decade. Evidence suggests that this is either because the soluble minerals were dissolved in the upper reaches and are not present in sediment in the lower reaches, or the water has dissolved as much of the minerals as possible. Thus, the lower river reaches are dominated by physical movement and not chemical modification of sediments.

1 Introduction

Roughly 1 x 10^9 tonnes of sediment per year are eroded from the Himalaya and transported through the Ganges-Brahmaputra-Meghna (GBM) delta (Milliman & Farnsworth, 2013). Chemical weathering of silicates in these sediments and subsequent precipitation of carbonates is hypothesized to have caused drawdown of atmospheric CO_2 and global cooling in the Cenozoic (Raymo & Ruddiman, 1992) and to increase seawater $^{87}Sr/^{86}Sr$ over the last 40 Ma (Edmond, 1992). Recent studies have found that chemical weathering of sediments occurs not just in the Himalayan source and in rivers, but also in the upper delta floodplain (Bickle et al., 2018; Lupker, France-Lanord, et al., 2012). This region is "weathering limited" because the rate of chemical weathering is limited by kinetic and climatic factors and not by the supply of unweathered sediment. Because the rate of sediment supply is high due to rapid exhumation and erosion in the Himalayan source, the rate of chemical weathering is high. Readily weathered minerals such as plagioclase persist in the floodplain, and weathering causes measurable changes in the composition of suspended sediments (Lupker, France-Lanord, et al., 2012) and dissolved loads (Bickle et al., 2018) in the Ganges upstream of Harding Bridge in Bangladesh. Chemical weathering rates should decrease downstream as the rate of supply of unweathered primary minerals slows until a transport-limited regime is reached in the lower Ganges tidal plain, as hypothesized by Bickle et al. (2018), but this has not been tested. In this study the compositions of rice paddy soils with approximately known ages, and tidal channel sediments are compared to qualitatively assess the rate of chemical weathering in the Ganges tidal delta plain in Southwest Bangladesh, ~340 km downstream from

Harding Bridge (Fig. 1). A small number of upstream and downstream tidal channel water samples are also compared to see if floodplain weathering in the tidal plain contributes dissolved solutes. We also evaluated the mobilities of major and trace elements by measuring apparent distribution coefficients of 22 elements between solids and coexisting water or deionized water extracts, and investigated spatial and seasonal influences.

1.1 Setting

Bangladesh has a tropical, seasonal climate, with 80% of rainfall occurring during the monsoon from June to September (N. T. Chowdhury, 2010). The coastal region of Southwest Bangladesh consists of polders, islands surrounded by and separated from tidal channels by embankments. The tidal channels experience large seasonal changes in water salinity from ~0 ppt in the wet season to an average of ~15 ppt in the dry season for our study area (Ayers et al., 2017). Salinity can also vary on a diurnal and biweekly cycle, with higher salinity at spring high tide due to the increased proportion of seawater from the Bay of Bengal (Ayers et al., 2017). Tidal channels are the primary source of irrigation water in this region, because the local groundwaters are largely saline (Benneyworth et al., 2016; Naus et al., 2019). In the wet season when tidal channels are fresh, farmers grow rice in paddies, while in the saline dry season some switch to brine shrimp aquaculture, while others with access to fresh groundwater use it to irrigate rice paddies (Barmon et al., 2010).

The region of study is in the western portion of the lower GBM delta (Fig. 1). Besides intensively cultivated polders, it includes the Sundarbans National Forest, the world's largest littoral mangrove forest (Hale et al., 2019). The study area is an abandoned lobe of the delta, largely cut off from the main Ganges river stem and dominated by tidal deposits. In this Ganges tidal delta plain, the deposits are considered estuarine because there is a net landward transportation of sediment that is mostly sourced from the mouth of the GBM river by way of the inner shelf (M. Allison & Kepple, 2001; Rogers et al., 2013). About half of the deposits are transported directly from the river mouth along the shelf and then inland by the tides, while half is from upstream reworked deposits (Rogers et al., 2013). Tidal deltaic deposits define the surficial geology, with upper silt and clay thicknesses from just a few meters up to 20 to 30 meters (MA Allison et al., 2003; Ayers et al., 2016). No previous studies have investigated how the composition of these deposits change after deposition.

1.2 Factors influencing compositions of solids

The mineralogy and chemical composition of sediments deposited by rivers depends on source characteristics; grain size sorting resulting from hydraulic effects, such as selective entrainment and settling; and chemical weathering during transport (Garzanti et al., 2010, 2011). In the Ganges River basin the chemical composition of sediments primarily depends on mineral sorting and, therefore, grain size and density, and secondarily on depletion of mobile elements by chemical weathering in the floodplain (Lupker, Blard, et al., 2012). In the Sundarbans, where sediment deposition is unaffected by human activity, the median grain size is 31 μm (medium silt) near the Sutarkhali tidal river, decreases inland, and does not change seasonally (R P Hale et al., 2019).

Tidal islands in SW Bangladesh were converted to polders in the 1960s by building embankments. This reduced the frequency of flooding and, therefore, the sediment deposition rate on the polders (Auerbach et al., 2015). Today, tidal channel sediments are deposited on polders only when embankments are breached deliberately for tidal river management (Gain, 2017), when sluice gates are temporarily opened, or by storm surges that breach the embankments. For example, in 2009 Cyclone Aila caused long-term tidal flooding on Polder 32 due to embankment failures, which is a key area of this study (Fig. 1). This caused an elevated mean sediment deposition rate of 17.8 cm/yr (Auerbach et al., 2015). In contrast, the natural background rate of sedimentation at Polder 32 indicates average Holocene deposition of ~0.6-0.8 cm/y (Ayers et al., 2016). This compares well to modern measurements in the Sundarbans that yield average annual sediment deposition (vertical accretion) rates of ~1 cm/y (Rogers et al., 2013), but with seasonality, from ~0.9 cm/y in the dry season to 1.2 cm/y in the wet season for island interiors (Bomer et al., 2020). We use these deposition rates to estimate mean elapsed time since sediment deposition, and thus the amount of time rice paddy soils were exposed to chemical weathering.

The silt-sized sediments deposited on polders are transported in tidal channels as suspended sediment. Studies of Ganges River sediments show that suspended sediment mineralogy and composition in the Ganges depends primarily on grain size, which varies from fine to medium silt at the surface to coarse silt and fine sand above the channel bed (Garzanti et al., 2011). Common minerals include quartz, feldspar, mica, calcite, dolomite, and epidote-amphibole-garnet suites, with slow-settling phyllosilicates and the elements they host concentrated near the surface (Garzanti et al., 2011). However, about half of the sediment deposited in the tidal delta plain is currently sourced from the Bay of Bengal through tidal exchange, and includes sediments derived from the Brahmaputra, Meghna, and Ganges Rivers (Rogers et al., 2013; R. P. Hale et al., 2019). When first deposited on polders, sediments are likely to

inherit the texture, mineralogy, and composition of suspended sediments as the tidal river overtops or breaches the embankment.

The main pedogenic processes that convert sediment to soil in low-lying regions such as SW Bangladesh are (i) homogenization through bioturbation, (ii) mechanical weathering by plant roots, (iii) oxidation-reduction processes of Fe and Mn, (iv) accumulation of organic matter, (v) conversion of primary to secondary minerals such as clays through acid hydrolysis, and (vi) base leaching from calcareous top soils (Hugh Brammer, 2016; Chen et al., 2011). Oxidation of iron under aerobic conditions produces rust colored soils, whereas the reduction of iron when soil is saturated and anaerobic produces grey colored soils (Horneman et al., 2004). Rice paddy soils in the tidal delta plain are often exposed to aerobic conditions in the dry season and anaerobic conditions in the wet season due to waterlogging, resulting in the formation of both rust and grey colored patches in soils (Brammer, 2016). In 2012 on Polder 32 we observed laminations in pits excavated for ponds. These laminations formed by daily tidal inundation following the breach of embankments during Cyclone Aila in 2009 (Auerbach et al., 2015). Soil horizon development was not observed, indicating the soils were entisols (Fry, 2015) and that sediments remained relatively unaltered at least three years after deposition.

1.3 Chemical Weathering in the Ganges Basin

Previous studies of river chemistry in this region have shown that carbonate weathering dominates during the monsoon due to faster dissolution kinetics, while silicate weathering dominates in the dry season due to longer water-rock interaction times and a greater proportion of groundwater baseflow with high solute content (Tipper et al., 2006). In weathering-limited areas in the upper reaches of large watersheds, rates of exhumation, erosion, and chemical weathering are high and fluid residence times are short (Maher, 2010). In the upper reaches of the Ganges Basin, transported sediments are incompletely weathered, and floodplain weathering contributes a substantial fraction of weathering fluxes (Bickle et al., 2018; Lupker, France-Lanord, et al., 2012). However, no previous studies have explored chemical weathering rates in the lower reaches of the Ganges Basin. We hypothesize that in the Ganges tidal floodplain, chemical weathering rates should be transport-limited and lower than upstream in the alluvial fan and delta floodplain due to an inadequate supply of fresh sediment. In the tidal floodplain the rate of chemical weathering may also be low due to the presence of carbonate minerals in the commonly deposited calcareous alluvium – which buffer pH to alkaline values and limit the weathering of minerals by acid hydrolysis (Brammer, 2016) – and by the presence of swelling clays that make surface deposits impermeable (Benson et al., 1994). On the other hand, tilling and fertilization of rice paddy soil may accelerate the process of chemical weathering (Gandois et al., 2011).

1.4 Sampling Sites

Six sites chosen for this study spanned a wide range of surface water salinity and irrigation practices (Patton, 2018). Five sites were primarily used for agriculture, while one located in the Sundarbans mangrove forest represents natural background (Table 1, Fig. 1). The dominant soil type in this region is noncalcareous grey floodplain soil that is seasonally flooded and can develop deeper than 25 cm in noncalcareous alluvium (H Brammer, 2012). The soils on Polder 32 were deposited immediately after Cyclone Aila seven years before sample collection. For sites outside Polder 32 that were not inundated by Aila, the average time since deposition of the top 15 cm is less certain. Given that the long-term average regional sedimentation rate on polders is ~1 cm/y (Rogers et al., 2013), the average age of the top 15 cm would be ~7.5 years, not much different from the age of sampled deposits on Polder 32. However, it's unclear how much the relatively recent conversion of tidal islands to polders by addition of artificial levees, and their periodic breaching, has affected the average deposition rate, adding uncertainty to the age estimate.

2 Materials and Methods

2.1 Sample Collection and Field Measurements

Solid and water samples were collected at six sites (Fig. 1) in the dry season in May 2016 and wet season in November 2016 in order to describe spatial and temporal variations. Solid and water samples were collected from the same locations in rice paddies, tidal channels, and the Sundarbans. Rice paddy soil samples were collected from the uppermost 15 cm to represent the cultivated topsoil, or 'root zone' (Barmon et al., 2010). Rice paddy samples were collected from inundated paddies, while sample type "Dry Rice Paddy" was collected from a part of the paddy without standing water, usually in the dry season. We found that dry rice paddy samples were not significantly different in composition from rice paddy samples with standing water, so they are grouped together. Tidal channel sediment and water samples were collected from as close to the middle of the channel and mid-depth of the water

column as possible, usually from irrigation canals connected to tidal channels because the latter were too deep and wide for sampling. Roughly one kg of solid was collected for each sample.

A Decagon GS3 probe was used to measure soil moisture, temperature, and electrical conductivity in-situ in November 2016, and a Hach HydroLab DS5 Sonde was used to measure water temperature, pH, redox potential Eh, and specific conductivity (SpC) in-situ. Sample locations were recorded using a Trimble GeoXT 6000, with a horizontal accuracy of 50 cm.

Tidal channel water samples were collected from the middle of the channel and water column, while rice paddy water samples were collected from the middle of the water column. Water samples were collected by rinsing a one L bottle, filling it, and immersing a Hydrolab DS5 Sonde for field measurements. Rainwater samples were collected in clean glass dishes set out just before a rain event. Next, a syringe was used to withdraw 30 mL from either a one L bottle after field measurements, or a clean glass dish. Water was then filtered at 0.45 μm into a polyethylene sample bottle. One drop of concentrated nitric acid (HNO_3) was added to the bottle before Inductively Coupled Plasma (ICP) analysis. Another 60 mL was filtered and placed in a sample bottle without acid for Ion Chromatography (IC) and Total Organic Carbon (TOC) analysis.

2.2 Sample Preparation

Solid samples were air dried, sieved with a No. 10 sieve, and homogenized by powdering in a mortar and pestle. Two to three grams were used to measure loss on ignition (LOI) at 105°C for H_2O- (adsorbed water) content and 1000°C for H_2O+ (structural water) content in an alumina crucible (Pansu & Gautheyrou, 2007). A second split for extract preparation was dried at 110°C. Ten grams of solid was weighed and added to 50 mL of deionized water to form a slurry. The slurry was stirred for 15 minutes, then measured for pH using an Accumet pH meter and SpC using a HANNA Portable Solution Conductivity Measurement Meter (Tan, 2005). The saturated slurries were then filtered using a vacuum pump, coarse porosity/fast flow filter paper, and a Büchner flask and funnel. The extracts were filtered for a second time through a 0.45 μm syringe filter. Fifteen mL was placed in a conical vial, and 300 uL of concentrated nitric acid was added to make a 1% HNO3 acid solution for ICP analysis. Another 30 mL was saved unacidified for IC and TOC analysis. All water and extract samples were refrigerated until analysed.

After LOI measurement, lithium metaborate ($LiBO_2$) fusion was completed using the same solid samples to measure their bulk composition. One hundred mg of solid sample and 600 mg $LiBO_2$ powder were weighed using an analytical balance and then mixed with an agate mortar and pestle under acetone. The mixture was air dried and transferred using weighing paper to a new graphite crucible. The crucible was then placed in a preheated oven for 10 minutes at 1100°C. The molten bead that had formed was poured into 50 mL of hot 1 molar (M) nitric acid (HNO_3) and stirred until the solid material was no longer visible (a minimum of 5 minutes). The cooled sample was transferred to a 50 ml centrifuge tube and brought to a volume of 50 mL by adding 1 M HNO_3.

2.3 Laboratory Analysis

Samples of water, extracts, and dissolved solids were analyzed using methods described in Ayers et al. (2016), who also list method detection limits. Anions were measured in water and extract samples using ASTM Method D-4327-03 on a Metrohm 881 Compact IC Pro. Dissolved inorganic carbon (DIC) and dissolved organic carbon (DOC) were measured in water and extract samples using ASTM Method D-7573-09 on a Shimadzu model TOC-V CPH/CPN. Major cations were analyzed for using EPA Method 6010B on a Varian ICP Model 14720-ES ICP-OES. Trace metals were measured using a Perkin Elmer model ELAN DRC II ICP in both standard and dynamic reaction chamber (DRC) modes.

Select solid samples were analyzed for particle size using a Malvern Mastersizer 2000. A homogeneous subset of each solid sample analyzed was placed in a 1 L beaker of deionized water after running deionized water through the instrument to establish background concentrations. Sample were then deflocculated while suspended in deionized water via sonication before analysis. Samples were analyzed for the grain size range of 0.563 μm to 1.27 mm.

Minerals in select solid samples were identified using powder x-ray diffraction at Vanderbilt University. Dried, homogenized powder samples were dry cast on 20 x 20 mm square sample glass holders with a 0.2 mm indent and analyzed with a Rigaku SmartLab powder X-ray diffractometer with a Cu source of X-rays with a Kα wavelength of 0.154 nm at 40 kV and 44 mA. The detector was a D/teX Ultra 250 1D silicon strip detector. PDXL software identified the mineral phases associated with the intensity peaks.

Saturation index calculations were performed using the Spec8 program in Geochemists Workbench v.8 with the default thermo.dat database (Bethke, 2007). Data analysis was performed in R (R Core Team, 2019). Spatial analysis was conducted using ArcGIS Pro.

2.4 Quality Assurance/Quality Control

Deionized water was used for water sample blanks to test for water contamination in the field, and replicates of select samples were collected in order to quantify precision. Water samples were kept refrigerated and were analyzed less than one month after collection. Our previous work has shown that, except for nitrate ions, measured concentrations do not change for at least one month after sample collection (Ayers et al., 2017). Charge imbalance errors for water samples averaged 4.1%, with the maximum being 21%. Measured concentrations for species reported here were well above the method detection limit (given in Ayers et al., 2016) for most elements, and sample concentrations were always significantly higher than blank concentrations. For replicate water samples, the average percent difference in measured major element concentrations was 1.6%, indicating good precision. For water samples, total dissolved solids calculated from chemical analyses showed excellent correlation with values measured using the Hydrolab (adj. $r^2 = 0.994$, n = 52). For extract solutions a comparison of major elements in duplicate sample analyses shows an average percent difference of 8.7%. Charge imbalance on extract analyses averaged 0.68%, with a maximum of 9.0%.

Bulk solid procedures were also performed using ≥ 99.9% SiO_2 to test for contamination. Except for SiO_2, oxide concentrations in these bulk solid blanks were on average 95% lower than concentrations measured in samples. USGS reference powders AGV-2 and GSP-2 were run as samples through the solid preparation procedures to test for accuracy, and duplicates were completed to quantify precision. Normalized AGV-2 major oxide concentrations were on average 12.6% different than the USGS reference, while GSP-2 oxides resulted in an average difference of 5.8%. Most trace element concentrations were within 20%. Duplicates show an average difference of 0.54% over all elements, indicating minimal error in sample preparation and analysis.

2.5 Estimation of Distribution Coefficients

The solid-water bulk distribution coefficient $D^{s/w}_i$ is defined as the concentration of element *i* in the solid C^s_i divided by that in the water C^w_i, both in ppm. $D^{s/w}$ values were estimated by analyzing water and solids collected at the same time and location. Only samples from rice paddies were included, as tidal channel water was rapidly flowing over tidal channel sediment and therefore unlikely to reach exchange equilibrium. Solid/extract $D^{s/e}_i$ values were estimated two ways. In the first, the measured bulk concentration of element *i* in the solid C^s_i was used with the measured concentration in the extract solution C^e_i, such that $D^{s/e}_i = C^s_i/C^e_i$. This assumes that the solid concentration was unaffected by equilibration with the extract solution. In the second method, the same information was used with mass balance to estimate the concentration in the residual solid C^{res}_i, which accounts for the amount of *i* that dissolved in the extract solution, as follows: $D^{s/e}_i = C^{res}_i/C^e_i$. Because measured $D^{s/e} >> 10$ for all elements, the concentration in the solid did not change significantly even for soluble elements, so calculating $D^{s/e}$ using the two methods yielded nearly identical results, but the more accurate values estimated using mass balance were used. $D^{s/e}$ values were estimated for all solid types: tidal channel sediment, rice paddy soil, and Sundarbans soil.

3 Data

Sample site locations are shown in Fig. 1 and listed in Table 1. Element concentrations grouped by sample type are tabulated for water samples (Table 2), extracts (Table 3), and solids (Table 4). Concentrations of the elements Be, Cd, Pb, and Tl were frequently below our method detection limits, and so are not reported. Furthermore, our procedure for analyzing solids prevented us from measuring sample concentrations of elements that mainly form anions (since the 1% HNO_3 solution could not be introduced into the ion chromatograph) or were present in the flux (Li and B). Concentrations reported as negative were deleted. Although some positive concentrations for the remaining elements were below the method detection limit, we chose to use the data uncensored with no substitution, as removing concentrations below the detection limit would bias the results to higher concentrations. Sample types included tidal channel (TC), rice paddy (RP), and Sundarbans (SB). Some samples classified as "tidal channel" were from irrigation canals connected to tidal channels.

For water samples collected in the same season (dry season in May and wet season in November), and extracts prepared from solid samples collected in the same season, element concentrations were most often lognormally distributed, as was reported for water samples from the same region by Ayers et al. (2017). All statistical tests and plots therefore use $\log_{10}$ values of concentrations. Although for solids many elements were not fit well by a lognormal distribution, we used a log transform on solid concentrations for consistency, and nonparametric statistical tests were used. Uncertainties are reported as one standard deviation (1σ).

Across sample sites, in-situ soil salinity slightly increased to the SE and with increasing proximity to the Bay of Bengal. In November, rice paddy water salinity slightly increased to the SSW. In general, soil and water salinity

decrease to the North and with increasing distance from the coastline. Although the sampling area was ~1300 km^2 (Fig. 1) and covered at least five different soil regions (Table 1), the variation in compositions of water and solid samples between sites was small within each season (e.g., Fig. S1), indicating similar processes are acting to transport elements across this region. We therefore lump data for all sites together in the following plots and discussion.

Values of specific conductivity (SpC), a proxy for salinity, of extracts were similar to in-situ solid conductivity measurements because the extract measurement was made on the solid slurry, not the filtered extract solution (Fig. 2). Salinity was much higher in solids and extracts than water samples (Fig. 2). Solids and extracts also show much less seasonality than water samples, which have higher salinity in the dry season.

To compare the wide range of element concentrations in solid, extract, and water, average concentrations were normalized to average upper continental crust (UCC) in spiderplots (Fig. 3) with elements arranged on the x-axis from lowest mobility during weathering and transport on the left to highest mobility on the right (Gaillardet et al., 2014). Tidal channel sediment (Fig. 3a) and rice paddy soil (Fig. 3b) are similar in composition to average UCC but depleted in Ca, Sr, Na, As, and S. Extract and water samples show strong depletions in immobile elements and weak depletions in the mobile elements relative to solids. Extracts have higher concentrations than tidal channel and rice paddy water for most elements.

3.1 Water

In tidal channel water samples, variations in total dissolved solids (TDS) and SpC reflect variable contributions of seawater from the Bay of Bengal (Ayers et al., 2017). Calculated TDS in water samples ranged from 20 ppm in rainwater to as high as 20,276 ppm in May tidal channel samples. Tidal channel water has much higher salinity in the dry season than the wet season (Fig. 2). Wet season tidal channel and rice paddy water have similar salinity and element concentrations, consistent with observed irrigation of rice paddies with tidal channel water in the wet season (Ayers et al., 2017). In the dry season, most rice paddies have lower salinity than tidal channel water because they are irrigated with groundwater. Concentrations of conservative elements, which show a constant ratio with Cl concentrations, are consistent with these relationships inferred from salinity. Immobile elements such as Al, Fe, Zn, and Cr show little variation in concentration by season or location (as measured by the size of the error bars in Fig. 3), while redox sensitive elements such as Mn and S show larger variations (Table 2).

Saturation index calculations on seasonal average water compositions show that rice paddy and tidal channel waters are always saturated in hydroxyapatite, dolomite, muscovite, and the smectite mineral saponite, and usually saturated in illite, kaolinite, calcite, and K-feldspar. Dry season waters are also saturated in the smectite mineral beidellite.

3.2 Extracts

Like water, extracts show little variation in concentrations of immobile elements such as Al, Fe, Zn, Cr, and Ni by season or location (Table 3, Fig. 3). Soluble elements such as Na and redox sensitive elements such as Mn and S show relatively large seasonal variations. Extracts from tidal channel sediments collected in the dry season generally have higher concentrations and SpC values than wet season extracts, though the same is not true for rice paddy samples. Extract pH was nearly always > 7.5 with little seasonal variation, consistent with the presence of carbonate minerals. Sundarbans and tidal channel sediment samples have higher extract TDS and SpC than rice paddies, suggesting that agricultural activity may flush out soluble salts (Fig. 2).

Comparison of sulfur in extracts measured as elemental S by ICP-OES and sulphate SO_4^{2-} measured by IC shows the two are highly correlated (r = 0.997). The median molar concentration was higher for S measured by ICP-OES at 6.4×10^{-4} than SO_4^{2-} measured by IC at 6.1×10^{-4}, suggesting a small portion was present as sulfide, and that most S is present as sulphate.

Saturation index calculations show that rice paddy soil and tidal channel sediment extracts are always saturated in hydroxyapatite and kaolinite, and usually saturated in illite, gibbsite, smectite minerals beidellite and saponite, and dolomite ± quartz and calcite. Extracts are undersaturated in hydrous ferric oxyhydroxides that often control the mobility of arsenic and other elements in this region (Hossain et al., 2012). This may be due to their absence in the solids, to disequilibrium, or to their abundance being less than required to saturate the volume of extract solution.

3.3 Solids

The composition of sediment is strongly influenced by grain size (Garzanti et al., 2011). The mode, median, and volume-weighted mean grain sizes for select solid samples from this study are given in Table 5. The average

volume-weighted mean of rice paddy soils was 50 μm, tidal channel sediments 23 μm, and the single Sundarbans sample 48 μm. The median for the Sundarbans sample was 36 μm, similar to the 31 μm previously reported (R P Hale et al., 2019). We did not measure grain size distributions in enough samples to characterize spatial or seasonal variability. However, our limited measurements demonstrate that the sampled solids are dominantly silt-sized and roughly comparable in size, although the rice paddy soil samples are slightly coarser than the tidal channel sediment samples. Our tidal channel sediment samples are likely finer because they were collected from irrigation canals connected to the tidal channels. The lower flow velocity in the canals likely caused their bedload sediments to be finer than tidal channel bedload sediments and more similar to tidal channel suspended sediments.

Powder x-ray diffraction was used to identify minerals in two samples that were also characterized for grain size distribution: rice paddy soil sample BEMS_08_RPS_06M_May and tidal channel sediment sample BEMS_TC_01_May. Although the rice paddy sample is significantly coarser (Table 5), the minerals and their relative proportions assessed qualitatively by peak heights are very similar (Fig. 4). Quartz, illite, chlorite, biotite, and dolomite have multiple peaks in the 2θ range of 10-45°. Sample treatment is required to identify smectite. More detailed powder x-ray diffraction measurements have shown that in Ganges River sediments illite is the most abundant clay, followed by smectite, kaolinite, and chlorite (MA Allison et al., 2003; Khan et al., 2019).

Average tidal channel sediment and rice paddy soil concentrations of immobile elements are similar to those of UCC (Fig. 5). Converting to oxide concentrations and normalizing to an anhydrous basis again shows the similarities to UCC, although FeO is lower and CaO and MgO higher than UCC, most likely due to sediment sorting (Table 6). However, major elements with intermediate mobilities including Ca, Sr, and Na are depleted, likely due to depletion of plagioclase feldspar through sedimentary sorting or chemical weathering (Garzanti et al., 2011; Lupker, France-Lanord, et al., 2012). Mobile elements show variable behavior, with As and S being low relative to UCC. Compared to water and extracts, solid samples show less variation in element concentrations across seasons and sampling sites as measured by relative error bar size in Figs. 2 and 3.

Normalizing concentrations in rice paddy soil to tidal channel sediment highlights post-depositional changes in solid composition (Fig. 6). The only elements that show a substantial difference in concentration between rice paddy soil (C^{rp}) and tidal channel sediment (C^{tc}) were Na, with higher concentrations in May tidal channel sediment, and Si, which is higher in November rice paddy soil (Mann-Whitney test p values < 0.05). In both cases the 1σ error bars overlap with $\log_{10}C^{rp}/C^{tc} = 0$, indicating the differences in concentration are very small (Fig. 6).

4 Results

4.1 Element Correlations

Examination of element correlations can shed light on chemical processes. We found statistically significant correlations (p value for Pearson correlation coefficient < 0.05) for 160 of 406 element pairs in soil extracts (Figs. S3 and S4), 166/276 pairs in solids (Fig. S2), and 285/378 pairs in water. Log concentrations of conservative elements such as Na, Cl, K, Mg, and Sr in extract solutions are normally distributed and are all positively correlated, consistent with simple dissolution of soluble salts (Fig. S3). The same is true for water samples collected in this region in this study and previous studies (Ayers et al., 2017). In contrast, conservative elements do not always show good correlations in bulk solids (Fig. S2), which have much higher concentrations of all elements (except S) than water or extracts (Fig. 3). This indicates that only a small portion of most cations are present in solids as soluble salts, and generally cations remain bound to solid minerals such as clays during extract preparation or equilibration with standing water.

In contrast to conservative elements, log concentrations of nonconservative elements in water and extracts are not always normally distributed and can show positive, negative, or no correlation with other elements (Fig. S4). Arsenic shows a weak positive correlation with S in extracts, suggesting it may have been present in sulfides. However, if sulfide oxidation occurred during extract preparation, it was insufficient to reduce pH to < 7.

In bulk solids the metals Ba, Co, Cr, Cu, Fe, K, Mg, Mn, Na, Ni, Si, and Zn show strong ($r > 0.8$, $p < 0.05$) correlations with Al, indicating they are stored in clay minerals. Arsenic has a strong positive correlation with Fe ($r = 0.78$, $p = 2.6E\text{-}6$), suggesting it may be sorbed onto hydrous ferric oxyhydroxides (HFOs) (Fendorf et al., 2010). If HFOs are present, it is in abundance too low to detect by powder XRD or to saturate the extract solution. In tidal channel and rice paddy water samples, most elements show positive correlations with TDS, reflecting variable amounts of seawater mixing, dilution, and evaporative concentration.

4.2 Element Partitioning

In soils and sediments, weathering reactions between porewaters and minerals will cause dissolution of primary minerals, precipitation of secondary minerals, and adsorption onto mineral surfaces. Trace elements can be incorporated into solids through adsorption or coprecipitation/substitution. The partitioning of trace element *i* incorporated into multi-phase solids by substitution can be described using the solid-water bulk distribution coefficient, which has the same form as the linear adsorption isotherm: $D^{s/w}_i = C^s_i/C^w_i$. For trace elements, a plot of concentrations in water versus solid should yield a linear array with a positive slope and a zero intercept if Henry's Law is obeyed and solid mineralogy does not change, and the slope should equal the value of the trace element distribution coefficient $D^{s/w}$. This should be true regardless of whether the element is incorporated in solids by coprecipitation (substitution) or adsorption. While D values should be constant only for trace elements, they are still useful for evaluating whether major elements partition more strongly into solid or solution. $D^{s/w}$ values were calculated only for samples of water and rice paddy soil collected at the same time and location. $D^{s/e}$ values were calculated for extracts prepared from the same rice paddy soil or tidal channel sediment sample. D values are roughly lognormally distributed for each element. For most elements, $D^{s/w}$ values are similar to $D^{s/e}$ values (Fig. 7). D values calculated from average concentrations in Tables 2-4 are similar to averages from paired samples, suggesting our results are robust and not site-specific. Also, inter-element variances are larger than intra-element variances, suggesting that D values represent relative element mobilities (Fig. 7).

We observed poor and often negative correlations between concentrations of an element in solid and water or extract. The poor correlations may result from variable water compositions (especially pH) and solid mineralogies, although these would not likely cause negative correlations between concentrations in solids and aqueous solutions. Another potential explanation is disequilibrium partitioning. This is supported by seasonal changes in composition that are large for water and small for soil. From the dry season in May to the wet season in November, metal concentrations in soil and sediment change little (Fig. 5, larger error bars in Fig. 3 for water than for solids), despite surface water compositions changing dramatically from saline to fresh (Fig. 2). The average percentage seasonal difference in element concentrations were 147% and 13% for water and soil, respectively. Disequilibrium exchange is also supported by a lack of systematic dependence on pH, which should strongly affect mineral solubilities and adsorption of dissolved ions, and by the oversaturation of many minerals in extract solutions, including quartz. Also, the 15 minutes that the solid and extract solution remained in contact (the recommended duration for soil extracts cf. Tan (2005)) was likely insufficient to reach exchange equilibrium. Previous studies have shown that while > 75% of metal adsorption in batch experiments occurred within the first 30 minutes, some metals could take up to 300 minutes to reach a steady state solution concentration (Zhang et al., 2019).

While our measured distribution coefficients cannot be considered equilibrium D values, they are still useful as measures of element mobility and for identifying processes that affect element mobility. For sediments and soils in this region that have similar mineralogy, our D values can be used to estimate concentrations in solids from concentrations in standing water or extracts, which are easier to measure. This would be particularly useful for estimating concentrations of toxic elements such as As in agricultural soils.

As expected, D values are highest for the least mobile elements Al and Fe, and lowest for the most mobile element S (Fig. 7). Based on the mobility ranking (the order of elements on the x-axis), D is higher for Si and lower for Ca, Sr, and Na than expected. The higher D for Si is probably due to the relatively high proportion of quartz in the silt-sized sediments and soil (Fig. 4), while low D values for Ca, Sr, and Na likely result from removal of plagioclase feldspar by sedimentary sorting or weathering.

4.3 Sediment and Soil Compositions

Chemical weathering during transport and following sediment deposition converts primary minerals into dissolved solutes and secondary minerals, which changes the chemical compositions of solids and fluids. Weathering of sediments causes the following changes in mineralogy of sediments/soils and major element compositions of fluids: conversion of albite and K-feldspar to kaolinite or smectite releases Na and K respectively; conversion of biotite to vermiculite releases K; and calcite and dolomite dissolution release Ca and Mg (Lupker, France-Lanord, et al., 2012). Previous work has shown that progressive weathering of sediments near the Himalayan Front and the Ganges floodplain depletes sediments in the mobile elements that are released by weathering reactions (Lupker, France-Lanord, et al., 2012), particularly elements released by soluble minerals such as carbonates that dissolve rapidly. As a result, alkalis and alkaline earths in the suspended load of the Ganges River are depleted relative to UCC, even in the upper reaches of the Ganges Basin (Garzanti et al., 2011). We also observe depletion in alkaline earths like Ca and Sr and alkalis like Na, which could be caused by the removal of low-density plagioclase feldspar and its Na and

Ca components by chemical weathering (Fig. 5, Table 5, lack of plagioclase feldspar in x-ray diffraction patterns in Fig. 4). In contrast, tidal channel sediments and rice paddy soils both show enrichment in K relative to UCC (Table 5), probably due to illite being the most abundant clay mineral (Fig. 4).

At least half of the sediment deposited in the Ganges tidal plain is derived from the mouth of the main stem Meghna River (Rogers et al., 2013), which combines the drainage of the Ganges, Brahmaputra, and Meghna Rivers, which collect water and sediment from all the southern Himalaya. It is, therefore, not surprising that our sediment and soil samples from the Ganges tidal plain have trace element compositions very similar to average UCC (Fig. 3). However, plotting only solids highlights small differences between trace element concentrations in solids and UCC (Fig. 5). Compared to rice paddy soils and tidal channel sediments, normalized concentrations of many trace elements in Sundarbans soils are higher in the wet season and lower in the dry season (Fig. 5), although we have only one sample each of wet and dry season Sundarbans soils (cf. Table 4).

Poldering in coastal Bangladesh has greatly reduced the frequency of tidal flooding and sediment deposition. On Polder 32, the last significant sediment deposition event started with Cyclone Aila in 2009 and ended after embankment repairs were completed in 2010 (Auerbach et al., 2015). After roughly seven years, element concentrations in Polder 32 rice paddy soil are only slightly different from tidal channel sediment (Fig. 8), indicating little effect of in-situ chemical weathering.

Rice paddy soil and tidal channel sediment have similar mineralogy (Fig. 4), major element compositions (Table 6), and trace element compositions (Figs. 6 and 8). These similarities can only occur if two conditions are met: sediments deposited inside the polder are similar in composition to sediments deposited in the tidal channels/irrigation canals; and the influence of post-depositional weathering on mineralogy and composition is insignificant. Sediment deposition within polders occurred either before embankments were constructed in the 1960s or during tidal inundation following embankment breaches (Auerbach et al., 2015). None of the sampled areas have been affected by tidal river management, which involves deliberate flooding to induce sedimentation and an increase in land elevation to reduce waterlogging (Gain, 2017). Tidal inundation would cause deposition of silt-sized suspended sediments and not sand-sized bedload sediments within a polder, since silt is the dominant grain size in suspended sediments of most rivers (Garzanti et al., 2011), and is the dominant grain size in tidal channel sediments and polder soils within the study area (Table 5). Since polder soils have grain size distributions, mineralogies, and compositions similar to sediments deposited in tidal channels (although the measured polder soils were slightly coarser cf. Table 5), the effects of post-depositional chemical weathering within the polders have been insignificant. An alternative explanation is that since our tidal channel sediment samples were actually collected mostly from irrigation canals, the rice paddy soils are actually sediments deposited from irrigation water, and that this process is continuous. This could explain why our rice paddy soil and tidal channel sediment samples have similar mineralogies and compositions. However, our RP soil is coarser than the TC sediment, and if it was deposited by irrigation water, it would be finer. Furthermore, water in the irrigation canals moves very slowly due to miniscule changes in elevation, so that water entering rice paddies has near zero suspended sediment. If sediment deposition from irrigation water was significant, then irrigation canals would quickly clog with sediment, and rice paddies would be at higher elevation than adjacent land, neither of which was observed. Finally, a trench dug into surficial sediments inside Polder 32 showed that all near-surface sediment showed tidal laminations, indicating sediment was deposited during tidal inundation following Hurricane Aila.

A larger Bangladesh dataset of soil samples collected throughout Bangladesh showed that element concentrations in paddy and non-paddy soils are positively correlated and similar (M. T. A. Chowdhury et al., 2017). Linear regression of element concentrations in non-paddy versus paddy soils yielded a slope of less than one for all elements but arsenic, indicating that only arsenic was added to paddy soils by groundwater irrigation (M. T. A. Chowdhury et al., 2017). It is unclear whether the non-paddy soils in that study are comparable to tidal channel sediments in this study, but both studies demonstrate that the influence of rice paddy agriculture on soil composition in Bangladesh is small.

4.4 Chemical Weathering Rates

Our results suggest that element concentrations change more slowly in solids than in surface water as seasons change. Water-solid exchange rates must be too slow for solids to equilibrate with surface waters, which have short residence times and experience seasonal changes in composition. Solid exchange was also too slow to significantly modify the composition of the top 15 cm of soil on Polder 32 during the seven years between sediment deposition after Cyclone Aila in 2009 and our collection of rice paddy soils in 2016 (Fig. 8), although we see seasonal changes in concentrations of some elements, especially soluble salts (Table 4).

As discussed in Section 1.2, the average age of the top 15 cm at sites other than Polder 32 is estimated at ~7.5 years since deposition after Hurricane Aila in 2009 and sample collection in 2016. For polders other than Polder 32 that we collected samples from, it is possible that embankment breaches occurred during Hurricane Aila, but unlikely that they occurred after Aila and before sample collection. If Aila did not cause embankment breaches in these polders, then collected soil samples would be older than 7.5 years, since sedimentation rates in the region have decreased since poldering in the 1960s, but not by more than a few decades. During that time, chemical weathering had little effect on the composition of rice paddy soils at any of the investigated sites, indicating that the rate of chemical weathering is very low. The lack of a change in solid compositions across our field sites is mirrored by no significant change in November tidal channel water composition between upstream (4 samples from sites B3, B8, and B9) and downstream locations (4 samples from sites P32, B2, and SB), which are separated by ~ 50 km (Fig. 9). While changes in element discharge (solute fluxes) are needed to estimate the contribution from chemical weathering, the water discharge likely changes little over this 50 km stretch, so a lack of change in element concentrations is consistent with a lack of chemical weathering inputs. This is also supported by previous work in this region that found concentrations of conservative elements such as Na, Mg, Sr, and Cl in surface waters are explained by simple mixing of rainwater and seawater, with no contributions from chemical weathering (Ayers et al., 2017). The evidence suggests that most or all dissolved solutes in tidal channel water in the study area are derived from other areas, including the fluvial-dominated delta upstream and the Bay of Bengal downstream, and that chemical weathering rates in the study area are low.

Far upstream in the Ganges River Basin, in the Himalaya and the alluvial fan, weathering is rapid because exhumation and erosion provide a continuous supply of fresh sediments. In this weathering-limited regime in the headwaters of the Ganges, the chemical weathering rate is directly proportional to the physical erosion rate (Bickle et al., 2018; West et al., 2005), and river sediments show continuous downstream increases in the Chemical Index of Alteration, increases in clay concentrations at the expense of biotite and feldspar, and decreases in Th activity ratios and U/Th caused by chemical weathering (Granet et al., 2007). River waters in the upper reaches are less likely to be calcite-saturated than in the lower reaches (Sarin et al., 1989), while solute concentrations increase downstream from the alluvial fan before leveling off (Bickle et al., 2018). Sediment is weathered during transport as it works its way through the alluvial fan, which may be intermittent due to deposition and reworking in a braided stream network. In this weathering-limited regime, dissolved and suspended sediment fluxes increase downstream. Far upstream of our study area at Farraka, India, just upstream of Harding Bridge (Fig. 1), changes in Ganges River dissolved solute fluxes indicate that floodplain weathering contributes roughly half of major dissolved cation fluxes (Bickle et al., 2018), consistent with estimates based on sediment composition (Lupker, France-Lanord, et al., 2012). In contrast, in transport-limited areas the rate of chemical weathering is limited by the rate of supply of fresh material, and is lower than in the weathering-limited regime (Bickle et al., 2018; West et al., 2005). Our data suggest that a transport-limited regime prevails in the lower reaches of the Ganges Basin, consistent with predictions of a transition from weathering-limited regimes in highlands to transport-limited regimes in lowlands (Bickle et al., 2018; Gaillardet et al., 1999). In the lower river reaches, such as the tidal delta plain where our sampling sites are located, the solid material is more weathered than the fresh material in the alluvial fan. In the more intensely weathered sediment in the lower reaches, reactive/soluble primary minerals have mostly been replaced by secondary minerals such as clays, consistent with our observed sample mineralogies being dominated by the clay mineral illite and insoluble minerals such as quartz (Fig. 4). In the lowlands, water residence times are longer than in the highlands, especially in the floodplain, and tidal channel water that is used for irrigation has high dissolved solids, which lowers the chemical weathering rates of minerals. Water samples from rice paddies and tidal channels are saturated in the dominant minerals observed in our solid samples (illite, dolomite) and minerals that commonly occur in sediments in the lower reaches of the Ganges River basin (smectites and kaolinite), indicating that these minerals will not dissolve in the waters their host solids come in contact with. These waters are even saturated in primary minerals such as K-feldspar, muscovite, and hydroxyapatite. Extract solutions, which are likely more similar to soil porewater compositions than standing water in rice paddies, are even more concentrated in dissolved solutes, and saturated in the same minerals. The fact that water samples are already saturated in most of the minerals they would come in contact with is strong evidence that the driving force for chemical weathering is low. This explains our observed lack of change in soil composition over time (as compared with fresh tidal channel sediment), and lack of change in tidal river water composition across our study area. Somewhere between our downstream study area and Harding Bridge upstream must be the transition from weathering-dominated to transport-dominated regimes. For the main stem Ganges, the transition may be located near the break in river slope that separates the alluvial fan from the fluvial-tidal delta plain and causes a decrease in water velocity and average grain size downstream (Wilson & Goodbred, 2015).

Chemical weathering is transport-limited when there is a linear relationship on a logarithmic plot of physical erosion rate versus chemical weathering rate. These relationships are determined using mass discharge of dissolved solutes and sediments in main-stem rivers in the fluvial-dominated part of the delta (Bickle et al., 2018). Our study area is in the tidal floodplain, where it is less clear what physical erosion rate means, and which we have not measured. However, our data show that the chemical weathering rate in the tidal delta plain is low, which is more consistent with a transport-limited regime than a weathering-limited regime. The area of the delta in the transport-limited regime should increase with factors that increase the rate of chemical weathering such as temperature and runoff (West et al., 2005). Since both of these factors are high in the GBM delta, it seems likely that the entire tidal delta plain is in the transport-limited regime.

The instantaneous weathering rate of solid material decreases with increasing time spent in the weathering environment. The residence time of organic carbon in river sediments in the upstream fluvial-dominated part of the Ganges Basin in Bangladesh is ~2 kyr on average (Galy & Eglinton, 2011). This suggests that much of the sediment was stored in the floodplain for over one thousand years, so that dead organic matter could accumulate in soil before reworking released it to the river. The amount of time elapsed since physical erosion in the Himalaya to deposition is even greater than one thousand years for the tidal floodplain, since much of the sediment was transported all the way to the Bay of Bengal, potentially stored there for a significant amount of time, and then transported inland by the tides before deposition. Thus, by the time sediments are deposited in our field area, they have been thoroughly weathered.

While the older sediment ages and higher solute loads in the tidal delta plain decrease the Gibbs Free Energy change and rates of chemical weathering reactions, the lack of systematic partitioning (and the oversaturation in many minerals) shows that solids and surface waters are not in chemical equilibrium. Solids show little seasonal variation in composition, while surface waters show large variations. Disequilibrium between standing water and the top 15 cm of sediment and soil may result from the solids being dominated by swelling clays such as smectites that are abundant in the Ganges clay-sized fraction (Borromeo et al., 2019) and that make surface deposits impermeable (Benson et al., 1994). Swelling will occur in the wet season due to abundant water for interlayer sites in smectites such as beidellite, while in the dry season abundant Na^{+} may displace Ca^{2+} and Mg^{2+} and cause swelling (Langmuir, 1997). Swelling clays may therefore inhibit chemical weathering reactions in the soil.

5 Conclusions

Rice paddy soil and tidal channel sediment in the Ganges tidal plain in SW Bangladesh have similar mineralogies and compositions. Since soils formed from tidal channel sediments deposited at least 7.5 years ago, the lack of change in composition during that time indicates low rates of chemical weathering characteristic of a transport-limited regime, in contrast with the documented weathering-limited regimes > 340 km upstream (Bickle et al., 2018; Lupker, France-Lanord, et al., 2012). Rice paddy and tidal channel waters are saturated in the dominant minerals present in soils and sediments, indicating low Gibbs Free Energy changes and rates of weathering reactions.

Tidal channel sediment and rice paddy soil show little or no seasonal variation in composition. In contrast, the composition of water in rice paddies and tidal channels does vary seasonally, with wet season samples being more dilute. This suggests that compositions of solids change more slowly than solutions, which explains much of the intra-element variation in our measured apparent solid/water distribution coefficients. While measured distribution coefficients are not equilibrium values, the relative values for the elements studied are mostly consistent with previously published trends of element mobility during weathering and transport (Gaillardet et al., 2014), and values can be used with measured water compositions to estimate compositions of soils and sediments with similar mineralogies. Disequilibrium partitioning between fine-grained sediments and surface waters may be a common feature in river deltas due to the presence of swelling clays, the low supply of unweathered material, and saturation of most available minerals in water, which together keep chemical weathering rates low.

Acknowledgments, Samples, and Data

The authors have no financial conflicts of interested related to this paper. Thanks to Steve Goodbred for advice, Rossane DeLapp for quickly analyzing our samples, Md Nazrul Islam (Bachchu) from Pugmark Tours, Saddam Hossain from Dhaka University, and Chelsea Peters from Vanderbilt University for help in the field. Any opinions, findings, conclusions, or recommendations expressed in this material are those of the authors and do not necessarily reflect the views of the National Science Foundation.

Research Data associated with this article can be accessed at http://dx.doi.org/10.17632/6z6bdxrkkb.2

References

Allison, M., & Kepple, E. (2001). Modern sediment supply to the lower delta plain of the Ganges-Brahmaputra River in Bangladesh. *Geo-Marine Letters*, *21*(2), 66–74. https://doi.org/10.1007/s003670100069

Allison, MA, Khan, S., Goodbred, S., & Kuehl, S. (2003). Stratigraphic evolution of the late Holocene Ganges–Brahmaputra lower delta plain. *Sedimentary Geology*, *155*, 317–342. https://doi.org/10.1016/S0037-0738(02)00185-9

Auerbach, L. W., Goodbred Jr, S. L., Mondal, D. R., Wilson, C. A., Ahmed, K. R., Roy, K., et al. (2015). Flood risk of natural and embanked landscapes on the Ganges–Brahmaputra tidal delta plain. *Nature Climate Change*, *5*(2), 153–157. https://doi.org/10.1038/nclimate2472

Ayers, J. C., Goodbred, S., George, G., Fry, D., Hornberger, G., Benneyworth, L., et al. (2016). Sources of salinity and arsenic in groundwater in southwest Bangladesh. *Geochemical Transactions*, *17*(4), 1–22. https://doi.org/10.1186/s12932-016-0036-6

Ayers, J. C., George, G., Fry, D., Benneyworth, L., Wilson, C., Auerbach, L., et al. (2017). Salinization and arsenic contamination of surface water in southwest Bangladesh. *Geochemical Transactions*, *18*(1), 4. https://doi.org/10.1186/s12932-017-0042-3

Barmon, B. K., Kondo, T., & Osanami, F. (2010). Rice-prawn Farming System: Impacts on Soil Quality and Land Productivity of Modern Variety Paddy Production in Bangladesh. *Asian Journal of Agriculture and Development*, *7*(2), 49–66. Retrieved from http://beta.searca.org/searca/ajad/files/101111132631_Barmon, Kondo, Yamaguchi, and Osanami.pdf

Benneyworth, L., Gilligan, J., Ayers, J., Goodbred, S., George, G., Carrico, A., et al. (2016). Drinking water insecurity: water quality and access in coastal south-western Bangladesh. *International Journal of Environmental Health Research*, *26*. https://doi.org/10.1080/09603123.2016.1194383

Benson, C. H., Huaming, Z., & Xiaodong, W. (1994). Estimating Hydraulic Conductivity of Compacted Clay Liners. *Journal of Geotechnical Engineering*, *120*(2), 366–387. https://doi.org/10.1061/(ASCE)0733-9410(1994)120:2(366)

Bethke, C. M. (2007). *Geochemical and biogeochemical reaction modeling*. Cambridge University Press.

Bickle, M. J., Chapman, H. J., Tipper, E., Galy, A., De La Rocha, C. L., & Ahmad, T. (2018). Chemical weathering outputs from the flood plain of the Ganga. *Geochimica et Cosmochimica Acta*, *225*, 146–175. https://doi.org/https://doi.org/10.1016/j.gca.2018.01.003

Bomer, E. J., Wilson, C. A., Hale, R. P., Hossain, A. N. M., & Rahman, F. M. A. (2020). Surface elevation and sedimentation dynamics in the Ganges-Brahmaputra tidal delta plain, Bangladesh: Evidence for mangrove adaptation to human-induced tidal amplification. *CATENA*, *187*, 104312. https://doi.org/https://doi.org/10.1016/j.catena.2019.104312

Borromeo, L., Andò, S., France-lanord, C., Coletti, G., Hahn, A., & Garzanti, E. (2019). Provenance of Bengal Shelf Sediments: 1. Mineralogy and Geochemistry of Silt. *Minerals*, *9*, 640. https://doi.org/10.3390/min9100640

Brammer, H. (2012). *The Physical Geography of Bangladesh*. The University Press Ltd.

Brammer, Hugh. (2016). *Bangladesh: Landscapes, soil fertility and climate change*. Dhaka, Bangladesh: The University Press Limited.

Chen, L.-M., Zhang, G.-L., & Effland, W. R. (2011). Soil characteristic response times and pedogenic thresholds during the 1000-year evolution of a paddy soil chronosequence. *Soil Science Society of America Journal*, *75*(5), 1807–1820. https://doi.org/10.2136/sssaj2011.0006

Chowdhury, M. T. A., Deacon, C. M., Jones, G. D., Imamul Huq, S. M., Williams, P. N., Manzurul Hoque, A. F. M., et al. (2017). Arsenic in Bangladeshi soils related to physiographic region, paddy management, and mirco- and macro-elemental status. *Science of the Total Environment*. https://doi.org/10.1016/j.scitotenv.2016.11.191

Chowdhury, N. T. (2010). Water management in Bangladesh: an analytical review. *Water Policy*, *12*(1), 32. https://doi.org/10.2166/wp.2009.112

Edmond, J. M. (1992). Himalayan Tectonics, Weathering Processes, and the Strontium Isotope Record in Marine Limestones. *Science*, *258*(5088), 1594 LP – 1597. https://doi.org/10.1126/science.258.5088.1594

Fendorf, S., Michael, H. A., & van Geen, A. (2010). Spatial and temporal variations of groundwater arsenic in South and Southeast Asia. *Science*, *328*(5982), 1123–7. https://doi.org/10.1126/science.1172974

Fry, D. C. (2015). *Characterizing temporal and spatial trends in soil geochemistry on Polder 32, Southwest Bangladesh*. Vanderbilt University. Retrieved from http://etd.library.vanderbilt.edu/available/etd-07162015-214524/

Gaillardet, J., Dupré, B., Louvat, P., & Allègre, C. J. (1999). Global silicate weathering and CO2 consumption rates deduced from the chemistry of large rivers. *Chemical Geology*, *159*(1), 3–30.

https://doi.org/https://doi.org/10.1016/S0009-2541(99)00031-5
Gaillardet, J., Viers, J., & Dupré, B. (2014). Trace Elements in River Waters. In H. D. Holland & K. K. B. T. Turekian (Eds.), *Treatise on Geochemistry* (2nd ed., pp. 195–235). Oxford: Elsevier. https://doi.org/https://doi.org/10.1016/B978-0-08-095975-7.00507-6
Gain, A. (2017). Tidal river management in the south west Ganges-Brahmaputra delta in Bangladesh: Moving towards a transdisciplinary approach? *Environmental Science and Policy*, *75*(December 2016), 111–120. https://doi.org/10.1016/j.envsci.2017.05.020
Galy, V., & Eglinton, T. (2011). Protracted storage of biospheric carbon in the Ganges-Brahmaputra basin. *Nature Geoscience*, *4*(12), 843–847. Retrieved from http://dx.doi.org/10.1038/ngeo1293
Gandois, L., Perrin, A.-S., & Probst, A. (2011). Impact of nitrogenous fertiliser-induced proton release on cultivated soils with contrasting carbonate contents: A column experiment. *Geochimica et Cosmochimica Acta*, *75*(5), 1185–1198. https://doi.org/https://doi.org/10.1016/j.gca.2010.11.025
Garzanti, E., Andò, S., France-Lanord, C., Vezzoli, G., Censi, P., Galy, V., & Najman, Y. (2010). Mineralogical and chemical variability of fluvial sediments 1. Bedload sand (Ganga-Brahmaputra, Bangladesh). *Earth and Planetary Science Letters*, *299*(3–4), 368–381. https://doi.org/10.1016/j.epsl.2010.09.017
Garzanti, E., Andó, S., France-lanord, C., Censi, P., Vignola, P., Galy, V., & Lupker, M. (2011). Mineralogical and chemical variability of fluvial sediments 2. Suspended-load silt (Ganga–Brahmaputra, Bangladesh). *Earth and Planetary Science Letters*, *302*(1–2), 107–120. https://doi.org/10.1016/j.epsl.2010.11.043
Granet, M., Chabaux, F., Stille, P., France-Lanord, C., & Pelt, E. (2007). Time-scales of sedimentary transfer and weathering processes from U-series nuclides: Clues from the Himalayan rivers. *Earth and Planetary Science Letters*, *261*(3), 389–406. https://doi.org/https://doi.org/10.1016/j.epsl.2007.07.012
Hale, R. P., Wilson, C. A., & Bomer, E. J. (2019). Seasonal Variability of Forces Controlling Sedimentation in the Sundarbans National Forest, Bangladesh . *Frontiers in Earth Science* . Retrieved from https://www.frontiersin.org/article/10.3389/feart.2019.00211
Horneman, A., van Geen, A., Kent, D. V, Mathe, P. E., Zheng, Y., Dhar, R. K., et al. (2004). Decoupling of As and Fe release to Bangladesh groundwater under reducing conditions. Part I: Evidence from sediment profiles1 1Associate editor: G. Sposito. *Geochimica et Cosmochimica Acta*, *68*(17), 3459–3473. https://doi.org/https://doi.org/10.1016/j.gca.2004.01.026
Hossain, M., Williams, P. N., Mestrot, A., Norton, G. J., Deacon, C. M., & Meharg, A. A. (2012). Spatial heterogeneity and kinetic regulation of arsenic dynamics in mangrove sediments: The Sundarbans, Bangladesh. *Environmental Science and Technology*, *46*(16), 8645–8652. https://doi.org/10.1021/es301328r
Khan, M. H. R., Liu, J., Liu, S., Seddique, A. A., Cao, L., & Rahman, A. (2019). Clay mineral compositions in surface sediments of the Ganges-Brahmaputra-Meghna river system of Bengal Basin, Bangladesh. *Marine Geology*, *412*(September 2018), 27–36. https://doi.org/10.1016/j.margeo.2019.03.007
Langmuir, D. (1997). *Aqueous Environmental Geochemistry*. Upper Saddle River, NJ: Prentice Hall.
Lupker, M., Blard, P.-H., Lavé, J., France-Lanord, C., Leanni, L., Puchol, N., et al. (2012). 10Be-derived Himalayan denudation rates and sediment budgets in the Ganga basin. *Earth and Planetary Science Letters*, *333–334*, 146–156. https://doi.org/10.1016/j.epsl.2012.04.020
Lupker, M., France-Lanord, C., Galy, V., Lavé, J., Gaillardet, J., Gajurel, A. P., et al. (2012). Predominant floodplain over mountain weathering of Himalayan sediments (Ganga basin). *Geochimica et Cosmochimica Acta*, *84*, 410–432. https://doi.org/10.1016/j.gca.2012.02.001
Maher, K. (2010). The dependence of chemical weathering rates on fluid residence time. *Earth and Planetary Science Letters*, *294*(1), 101–110. https://doi.org/https://doi.org/10.1016/j.epsl.2010.03.010
Milliman, J. D., & Farnsworth, K. L. (2013). *River Discharge to the Coastal Ocean: A Global Synthesis*. *Cambridge University Press* (Vol. 24). https://doi.org/10.5670/oceanog.2011.108
Naus, F. L., Schot, P., Groen, K., Matin Ahmed, K., & Griffioen, J. (2019). Groundwater salinity variation in Upazila Assasuni (southwestern Bangladesh), as steered by surface clay layer thickness, relative elevation and present-day land use. *Hydrology and Earth System Sciences*, *23*(3), 1431–1451. https://doi.org/10.5194/hess-23-1431-2019
Pansu, M., & Gautheyrou, J. (2007). *Handbook of soil analysis: mineralogical, organic and inorganic methods*. Springer Science & Business Media.
Patton, B. (2018). *The Effect of Irrigation Source on Arsenic and Salt Concentrations in Soil in Southwest Bangladesh*. Vanderbilt University.
R Core Team. (2019). R: A Language and Environment for Statistical Computing. Vienna, Austria: R Foundation for Statistical Computing.
Raymo, M. E., & Ruddiman, W. F. (1992). Tectonic forcing of late Cenozoic climate. *Nature*, *359*(6391), 117–122.

https://doi.org/10.1038/359117a0

Rogers, K. G., Goodbred, S. L., & Mondal, D. R. (2013). Monsoon sedimentation on the "abandoned" tide-influenced Ganges-Brahmaputra Delta plain. *Estuarine, Coastal and Shelf Science*, *131*, 297–309.

Rudnick, R. L., & Gao, S. (2003). Composition of the continental crust. *Treatise on Geochemistry*, *3*, 659.

Sarin, M. M., Krishnaswami, S., Dilli, K., Somayajulu, B. L. K., & Moore, W. S. (1989). Major ion chemistry of the Ganga-Brahmaputra river system: Weathering processes and fluxes to the Bay of Bengal. *Geochimica et Cosmochimica Acta*, *53*(5), 997–1009. https://doi.org/https://doi.org/10.1016/0016-7037(89)90205-6

Tan, K. H. (2005). *Soil sampling, preparation, and analysis*. CRC.

Tipper, E. T., Bickle, M. J., Galy, A., West, A. J., Pomiès, C., & Chapman, H. J. (2006). The short term climatic sensitivity of carbonate and silicate weathering fluxes: Insight from seasonal variations in river chemistry. *Geochimica et Cosmochimica Acta*, *70*(11), 2737–2754. https://doi.org/https://doi.org/10.1016/j.gca.2006.03.005

West, A. J., Galy, A., & Bickle, M. (2005). Tectonic and climatic controls on silicate weathering. *Earth and Planetary Science Letters*, *235*(1), 211–228. https://doi.org/https://doi.org/10.1016/j.epsl.2005.03.020

Wilson, C. A., & Goodbred, S. L. (2015). Construction and maintenance of the Ganges-Brahmaputra-Meghna delta: Linking process, morphology, and stratigraphy. *Annual Review of Marine Science*, *7*, 67–88. https://doi.org/10.1146/annurev-marine-010213-135032

Zhang, J., Wang, X., Zhu, Y., Huang, Z., Yu, Z., Bai, Y., et al. (2019). The influence of heavy metals in road dust on the surface runoff quality: Kinetic, isotherm, and sequential extraction investigations. *Ecotoxicology and Environmental Safety*, *176*(March), 270–278. https://doi.org/10.1016/j.ecoenv.2019.03.106

720 # Tables

721 **Table 1.** Site locations and characteristics

Site	Latitude	Longitude	District	Thana	Union	Soil region[a]
B2	22.56895	89.58131	Bagerhat	Rampal	Rajnagar	**Eac:** Mixed Ganges River and Tidal Floodplains, non-saline
B3	22.86543	89.30501	Jessore	Keshabpur	Gaurighona	**Dba** or **Fcb**
B8	22.72527	89.19153	Satkhira	Tala	Khalishkhali	**Dba**: Old Southwestern Ganges River Meander Floodplains
B9	22.98833	89.48716	Jessore	Abhaynagar	Subha Para	**Fcb**: Old Floodplain Basins, Basin Margins
P32	22.50370	89.46009	Khulna	Dacope	Kamarkhola and Sutarkhali	**Ebc**: Southwestern Ganges Saline Tidal Floodplain
SB	22.45910	89.46735	Khulna	Dacope	Nalian Range	**Ebd**: Khulna Sundarbans Saline Tidal Floodplain

722 [a] Soil physiographic region (Brammer, 2016).
723
724
725

726 **Table 2**. Geometric mean element concentrations (mg/L) in water samples by sample type[a]

	RP-11 count	RP-11 geomean	RP-11 geosd	RP-5 count	RP-5 geomean	RP-5 geosd	SB-11 count	SB-11 geomean	SB-11 geosd	TC-11 count	TC-11 geomean	TC-11 geosd	TC-5 count	TC-5 geomean	TC-5 geosd
pH	34	8.25	1.07	14	7.97	1.06	2	7.85	1.01	8	7.7	1.03	5	7.25	1.04
SpC	34	1.02	2.38	14	5.64	2.86	2	1.63	1.51	8	1.73	2.24	5	12.5	6.02
Al	34	0.0297	1.35	14	0.0534	1.46	2	0.0298	1.1	8	0.0315	1.32	5	0.0546	1.64
As	34	0.00081	3.08	14	0.0083	2.58	2	0.00352	1.44	8	0.00327	2.5	5	0.00415	2.53
B	34	0.0834	2.37	14	0.262	2.67	2	0.291	1.06	8	0.169	2.65	5	1.15	3.5
Ba	34	0.521	3.08	14	0.175	2.12	2	1.93	1.59	8	2.21	2.13	5	0.138	3.74
Ca	34	42	1.4	14	146	2.49	2	43	1.24	8	51	1.32	5	145	2.22
Co	34	1.31E-05	2.31	14	0.000438	2.15	2	3.65E-05	1.26	8	3.64E-05	2.33	5	0.000333	4.06
Cr	34	0.000491	3.53	14	0.00146	1.35	2	0.00171	1.46	8	0.00143	2.41	5	0.00202	1.28
Cu	33	0.00143	2.2	14	0.00453	2.05	2	0.00215	1.83	7	0.00237	1.26	4	0.00908	3.04
Fe	32	0.000787	3.11	14	0.0257	2.97	2	0.000346	5.8	7	0.000712	1.89	5	0.00356	2.16
K	34	6.6	2.56	14	11	5.06	2	27.5	1.34	8	15.4	2.97	5	105	7.28
Mg	34	21.8	2.3	14	81.9	3.14	2	56.5	1.55	8	46.2	2.32	5	269	4.95
Mn	34	0.000724	3.47	14	0.11	5.68	2	0.00126	1.91	8	0.00115	2.03	5	0.0421	4.51
Mo	34	0.000139	2.2	14	0.00127	2.73	2	0.000661	1.28	8	0.000482	2.45	5	0.00361	2.51
Na	34	106	3.86	14	954	3.51	2	494	1.59	8	292	4.43	5	2100	9.92
Ni	34	0.000125	3.05	13	0.00425	2.11	2	0.000536	1.21	8	0.000185	9.13	5	0.00311	3.62
P	20	0.00785	2.94	14	0.194	3.75	2	0.00277	5.8	5	0.00663	2.34	5	0.0277	1.44
S	34	6.94	3.61	14	21.3	7.19	2	40.3	1.59	8	20.6	4.47	5	167	7.69
Sb	34	5.26E-05	1.72	14	0.000385	2.35	2	0.000125	1.9	8	0.000136	2.31	5	0.000475	1.36
Se	31	0.000111	8.98	14	0.000656	2.88	2	0.00224	1.75	7	0.00189	3.33	5	0.00116	4.52
Si	34	0.965	3.83	14	4.75	2.71	2	3.15	1.01	8	2.16	1.87	5	1.45	1.39
Sr	34	0.251	1.83	14	1	2.64	2	0.439	1.47	8	0.408	1.85	5	1.93	3.82
V	34	0.000752	2.22	14	0.013	1.78	2	0.00365	1.55	8	0.00265	3.11	5	0.0176	2.84
Zn	34	0.0343	1.21	13	0.0017	1.86	2	0.0351	1.4	8	0.0376	1.24	5	0.00607	4.48
Cl	34	160	4.05	14	1450	3.54	2	756	1.65	8	452	4.63	5	3150	9.91
Br	20	19.2	2.06	14	16.2	2.47	2	29.1	1.89	6	34.1	1.6	5	28.3	5.49
NO_3	3	2.58	1.49	5	1.07	5.4	0	0	0	1	2.05	0	1	0.138	0
DIC	34	31.6	1.36	14	47.1	1.69	2	34.7	1.58	8	29.9	1.27	5	26.3	1.17
DOC	34	33.1	1.28	10	70.6	1.4	2	34.5	1.56	8	14.4	2.96	3	37.2	1.26

727 [a] RP = rice paddy, TC = tidal channel, 11 = November, 5 = May, geomean = geometric mean, geosd = geometric standard deviation

728 **Table 3**. Geometric mean element concentrations in extracts by sample type, in ppm solid[a]

	RP-11 count	RP-11 geomean	RP-11 geosd	RP-5 count	RP-5 geomean	RP-5 geosd	SB-11 (n = 1)	SB-5 (n = 1)	TC-11 count	TC-11 geomean	TC-11 geosd	TC-5 count	TC-5 geomean	TC-5 geosd
pH	19	7.99	1.06	12	7.83	1.04	8.46	7.93	7	8.03	1.03	5	7.76	1.04
SpC	19	435	5.34	12	623	3	280	6010	7	2040	4.06	5	3940	3.6
Al	17	1.83	2.24	9	0.241	6.27	5.25	9.32	7	1.38	4.29	3	2.47	2.1
As	19	0.0284	1.82	13	0.0216	1.57	0.0252	0.0466	7	0.0282	1.88	5	0.0526	1.53
B	4	0.488	2.68	3	0.109	2.95			2	1.99	21.3	0		
Ba	19	0.133	1.75	13	0.133	1.36	0.062	0.231	7	0.158	1.93	5	0.318	2.21
Ca	17	71.6	2.74	12	145	1.57	28		5	224	7.04	2	637	4.64
Co	19	0.0016	4.29	10	0.000764	3.99	0.000497	0.00303	7	0.00185	2.59	5	0.00309	4.81
Cr	17	0.0131	2.89	13	0.00474	4.66	0.00935	0.0152	7	0.0104	2.32	4	0.0176	1.23
Cu	15	0.0537	2.58	12	0.0534	2.65	0.085	0.211	7	0.219	4.88	5	0.283	9.45
Fe	19	0	0	13	0.205	4.62	4.68	4.99	6	1.88	2.91	5	0.812	4.91
K	19	24.9	2.66	13	25.6	1.85	29.1	106	7	72.2	5.22	5	110	1.94
Mg	19	27.6	3.43	13	34.9	2.32	17.7	134	7	48.8	3.47	5	166	4.17
Mn	19	0.108	4.27	13	0.0993	3.31	0.046	2.49	7	0.675	7.6	5	2.73	4.36
Mo	19	0.0127	2.19	13	0.00943	1.75	0.0173	0.0209	7	0.0184	1.87	5	0.0202	1.85
Na	19	313	3.68	13	307	2.8	282	3770	7	1210	3.85	5	1500	5.61
Ni	19	0.017	1.82	13	0.0177	1.62	0.0137	0.018	7	0.0186	1.6	5	0.0303	1.75
P	14	0.265	2.47	11	0.266	2.5			3	0.843	2.08	2	0.472	3.96
S	19	98.8	4.68	13	54.5	2.51	104	391	7	224	2.98	5	581	3.24
Sb	19	0.00686	2.13	13	0.00514	1.85	0.00595	0.00321	7	0.0058	1.99	5	0.00518	1.72
Se	19	0.0175	2.03	12	0.0123	2.61	0.01	0.0493	7	0.0195	2.6	5	0.0533	4.75
Si	15	11.9	1.6	12	14.5	1.48	19.4		4	14.7	1.95	1	24.3	
Sr	18	0.366	2.64	13	0.556	1.58	0.147		5	1.65	8.93	4	1.91	3.45
V	19	0.026	1.86	13	0.0186	1.96	0.0221	0.0649	7	0.0256	2.32	5	0.0466	2.26
Zn	13	0.0331	3.7	11	0.0106	6.62	0.0105	0.76	5	0.41	4.7	4	0.794	1.27
Cl	19	469	3.71	13	462	2.85	425	5810	7	1800	3.77	5	2290	5.55
Br	9	26.4	1.9	3	38.3	5.56		22.6	5	17.9	1.97	4	28.2	2.14
NO3	6	8.26	3.39	8	29.5	4.19		2.78	2	2.07	1.02	5	3.03	2.11
DIC	19	43	2.22	13	53.8	1.5	61.7	51.9	7	51	1.61	5	47.5	1.25
DOC	19	244	1.49	13	229	1.42	206	196	7	213	1.58	5	305	1.69

729 [a] RP = rice paddy, TC = tidal channel, 11 = November, 5 = May, geomean = geometric mean, geosd = geometric standard deviation

730 **Table 4.** Concentrations in solid samples by sample type in ppm[a]

	Blank-5	RP-11 count	RP-11 geomean	RP-11 geosd	RP-5 count	RP-5 geomean	RP-5 geosd	SB-11 (n = 1)	SB-5 (n = 1)	TC-11 count	TC-11 geomean	TC-11 geosd	TC-5 count	TC-5 geomean	TC-5 geosd
Al	42.4	18	63800	1.23	12	57000	1.29	77800	32500	7	57100	1.35	6	59000	1.2
As	0.187	18	1.63	1.64	12	1.53	2.16	3.45	0.645	7	1.09	2.39	6	1.66	1.27
Ba	3.4	18	768	1.48	12	917	1.34	492	378	7	638	1.62	6	728	1.65
Ca	297	18	7600	1.7	12	11200	1.91	12300	9580	7	13400	1.38	6	10000	1.43
Co	0.214	18	11	1.55	12	8.19	1.54	12.2	8.45	7	8.56	1.59	6	8.95	1.25
Cr	3.81	18	55.3	1.22	12	47.9	1.48	94.1	18.2	7	39.7	1.83	6	51.5	1.24
Cu	3.65	18	29.4	1.31	12	27.5	1.71	37.5	23.4	7	27.3	1.38	6	28.3	1.46
Fe	75.4	18	30500	1.29	12	27200	1.48	47600	10900	7	25100	1.72	6	28900	1.21
K	203	18	36300	1.16	12	36100	1.25	33400	26700	7	33700	1.27	6	34800	1.28
Mg	58.1	18	10700	1.21	12	10000	1.29	13100	10500	7	11300	1.13	6	10600	1.17
Mn	2.25	18	432	1.4	12	408	1.35	693	417	7	592	1.25	6	455	1.09
Mo	2.37	18	1.96	2.05	12	1.8	1.82	12.5	0.945	7	1.84	2.02	6	1.28	1.88
Na	356	18	7990	1.29	12	8090	1.21	10700	11800	7	9530	1.28	6	9850	1.17
Ni	0.929	18	27.8	1.29	12	26.6	1.63	32.1	20.6	7	23.3	1.54	6	24.3	1.3
P	104	18	367	1.77	12	416	1.6	802	98.4	7	276	2.16	6	422	1.12
S	496	12	101	2.31	7	72.5	3.84	535	311	6	71.8	16.6	5	79.6	3.49
Sb	0.0453	18	0.249	2.63	12	0.356	1.99	0.379	0.0246	7	0.109	4.14	6	0.275	2.2
Se	1.31	5	0.0912	5.42	2	0.209	3.72			1	0.286		3	0.205	4.03
Si	241	18	227000	1.27	12	224000	1.19	330000	73700	7	167000	1.84	6	209000	1.11
Sr	0	18	82.9	1.19	12	84.3	1.19	121	88.7	7	95.8	1.15	6	82.4	1.18
V	5.59	18	73.1	1.48	12	78	1.36	103	21.6	7	40.5	2.55	6	72.7	1.25
Zn	1.3	18	77.8	1.21	12	72.2	1.32	83.4	53.7	7	70	1.21	6	73.5	1.16
H_2O^+		16	73700	1.18	10	78600	1.25	60000	61000	5	68600	1.23	5	73600	1.15
H_2O^-		16	23400	1.47	10	25200	2.26	22000	38000	5	19100	1.75	5	29000	2

731 [a] RP = rice paddy, TC = tidal channel, 11 = November, 5 = May, geomean = geometric mean, geosd = geometric standard deviation
732

Table 5: Measured grain sizes of select samples[a]

Sample Name	Median (μm)	Mode (μm)	Volume-Weighted Mean (μm)
BEMS_09_TC_01_Nov	16.37	14.98	28.44
BEMS_08_RP_06M_May	36.29	53.68	46.55
SB_SB_1_May	36.02	57.87	47.97
BEMS_03_RP_07_ Nov	21.41	23.15	43.16
BEMS_08_TC_01_ May	9.89	6.72	20.55
BEMS_08_RP_06M_ Nov	39.67	52.41	60.23
BEMS_08_TC_02_ May	22.95	34.62	30.33
BEMS_03_TC_01_ May	8.44	6.45	14.52

[a] Sample Name given as Site_Sample type_Sample #_Month. TC = tidal channel, RP = rice paddy, SB = Sundarbans

Table 6: Concentrations of oxides in solid samples[a]

Oxide	RP mean[b]	St Dev	TC mean	St Dev	Avg. UCC[c]	RP anhydrous mean	StDev	TC anhydrous mean	StDev
SiO_2	59.4	3.75	57.2	4.46	67.1	67.2	3.84	65.3	3.2
Al_2O_3	14	2.37	14.3	1.61	15.5	15.8	2.64	16.4	2.01
FeO	1.35	0.317	1.58	0.44	5.07	1.54	0.36	1.81	0.514
MgO	5.07	1.14	5.1	0.888	2.50	5.76	1.3	5.85	1.13
CaO	4.62	1.11	5.01	0.732	3.61	5.23	1.24	5.73	0.862
Na_2O	2.04	0.36	2.25	0.272	3.29	2.31	0.406	2.58	0.341
K_2O	1.46	0.87	1.91	0.869	2.82	1.66	1.02	2.17	0.938
P_2O_5	0.117	0.0368	0.121	0.0314	0.15	0.133	0.0409	0.139	0.036
H_2O^+	8.78	1.53	8.91	1.52					
H_2O^-	3.01	1.35	3.59	2.1					
Sum	100		100			100		100	

[a] Four samples with anomalously low SiO_2 were not included in these summary statistics. Concentrations of oxides normalized to 100%.

[b] Mean values are 5% trimmed mean, RP = rice paddy soil, TC = tidal channel sediment

[c] Rudnick and Gao (2003)

Figure Captions

Figure 1. Map of solid sample collection locations specified as Site_Sample #_Sample type. Water samples were collected from the same locations. The sample types are RP rice paddy, TC tidal channel, and SB Sundarbans. Detailed site maps are given in Figures S5-S8.

Figure 2. Boxplot comparing $\log_{10}$ of specific conductivity SpC in mS/cm of samples classified by group (rice paddy soil RP, Sundarbans SB, and tidal channel sediment TC), month (dry season May = 5, wet season November = 11), and sample type. In-situ solid SpC measurements were not made in May.

Figure 3. Average compositions of all solid, extract, and water samples normalized to average upper continental crust (Rudnick & Gao, 2003). The one standard deviation error bars represent the variability across sites, sample types, and season. Elements are arranged on the x-axis from lowest mobility during weathering and transport on the left to highest mobility on the right (Gaillardet et al., 2014). a) Tidal channel samples, n = 12 extract, 13 solid, and 13 water samples. b) Rice paddy samples, n = 32 extract, 30 solid, and 48 water samples. The red horizontal line represents average upper continental crust.

Figure 4. Powder x-ray diffraction patterns for rice paddy soil sample BEMS_08_RPS_06M_May in red and tidal channel sediment sample BEMS_TC_01_May in blue. The y-axis is observed intensity and is truncated for visualization.

Figure 5. Average compositions of rice paddy soil, Sundarbans soil, and tidal channel sediment in May and November. The horizontal red line represents average upper continental crust (Rudnick and Gao, 2003).

Figure 6. Concentration in rice paddy soil Crp normalized to concentration in tidal channel sediment Ctc by sample collection month, plotted as log values with one sigma error bars.

Figure 7. Log_{10} D values for solid/extract $D^{s/e}$ and solid/water $D^{s/w}$ with one sigma error bars. $D^{s/e}$ is an average of 29 rice paddy soil-extract pairs, 13 tidal channel sediment- extract pairs, and two Sundarbans soil- extract pairs, while $D^{s/w}$ is an average of 16 rice paddy soil-water pairs.

Figure 8. Average compositions of Polder 32 November samples of rice paddy soil and tidal channel sediment. No samples were collected in May. The horizontal red line represents average upper continental crust (Rudnick and Gao, 2003).

Figure 9. Comparison of average $\log_{10}$ concentrations in tidal channel water samples from upstream (4 samples from sites B3, B8, and B9) and downstream locations (4 samples from sites P32, B2, and SB).

Figure 1.

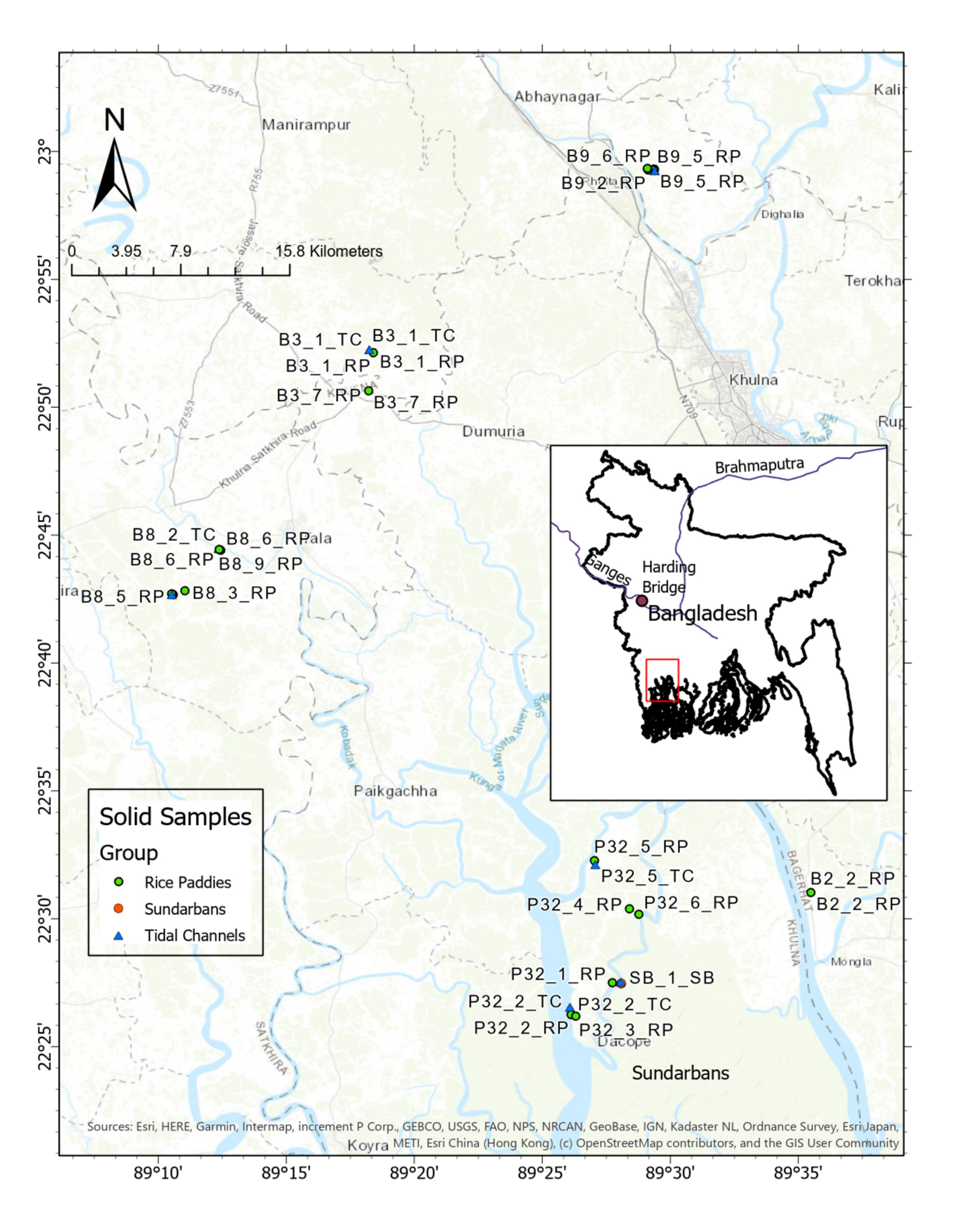
N
0 3.95 7.9 15.8 Kilometers
Abhaynagar
Manirampur
Dighalia
Terokha
Khulna
Dumuria
Paikgachha
Sundarbans
Koyra
Brahmaputra
Ganges
Harding Bridge
Bangladesh
B9_6_RP
B9_5_RP
B9_2_RP
B9_5_RP
B3_1_TC
B3_1_TC
B3_1_RP
B3_1_RP
B3_7_RP
B3_7_RP
B8_2_TC
B8_6_RP
B8_6_RP
B8_9_RP
B8_5_RP
B8_3_RP
P32_5_RP
P32_5_TC
P32_4_RP
P32_6_RP
B2_2_RP
B2_2_RP
P32_1_RP
SB_1_SB
P32_2_TC
P32_2_TC
P32_2_RP
P32_3_RP
Solid Samples
Group
Rice Paddies
Sundarbans
Tidal Channels
Sources: Esri, HERE, Garmin, Intermap, increment P Corp., GEBCO, USGS, FAO, NPS, NRCAN, GeoBase, IGN, Kadaster NL, Ordnance Survey, Esri Japan, METI, Esri China (Hong Kong), (c) OpenStreetMap contributors, and the GIS User Community
23°
22°55'
22°50'
22°45'
22°40'
22°35'
22°30'
22°25'
89°10'
89°15'
89°20'
89°25'
89°30'
89°35'

Figure 2.

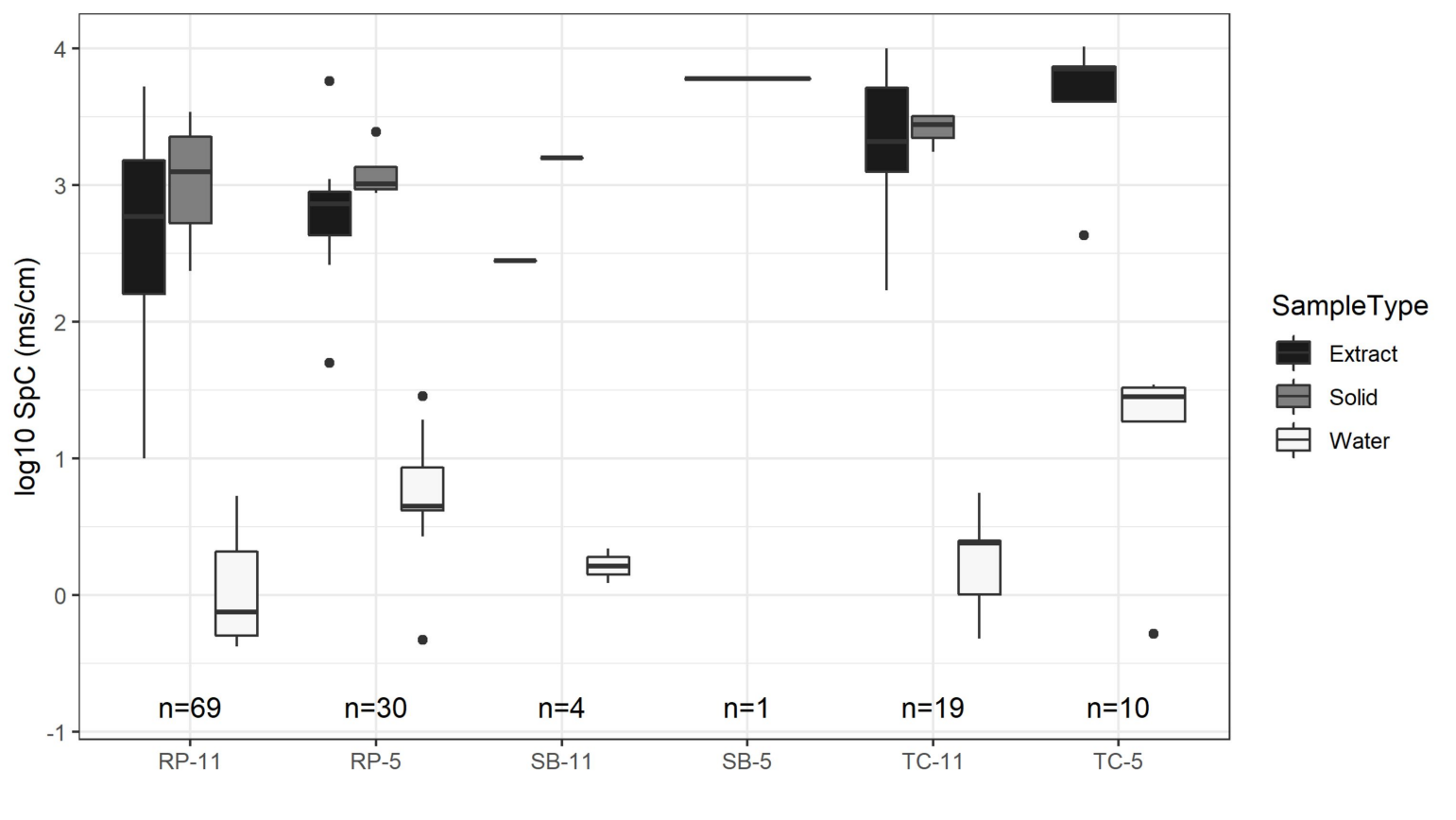
log10 SpC (ms/cm)
4
3
2
1
0
-1
n=69
n=30
n=4
n=1
n=19
n=10
RP-11
RP-5
SB-11
SB-5
TC-11
TC-5
SampleType
Extract
Solid
Water

Figure 3.

a)

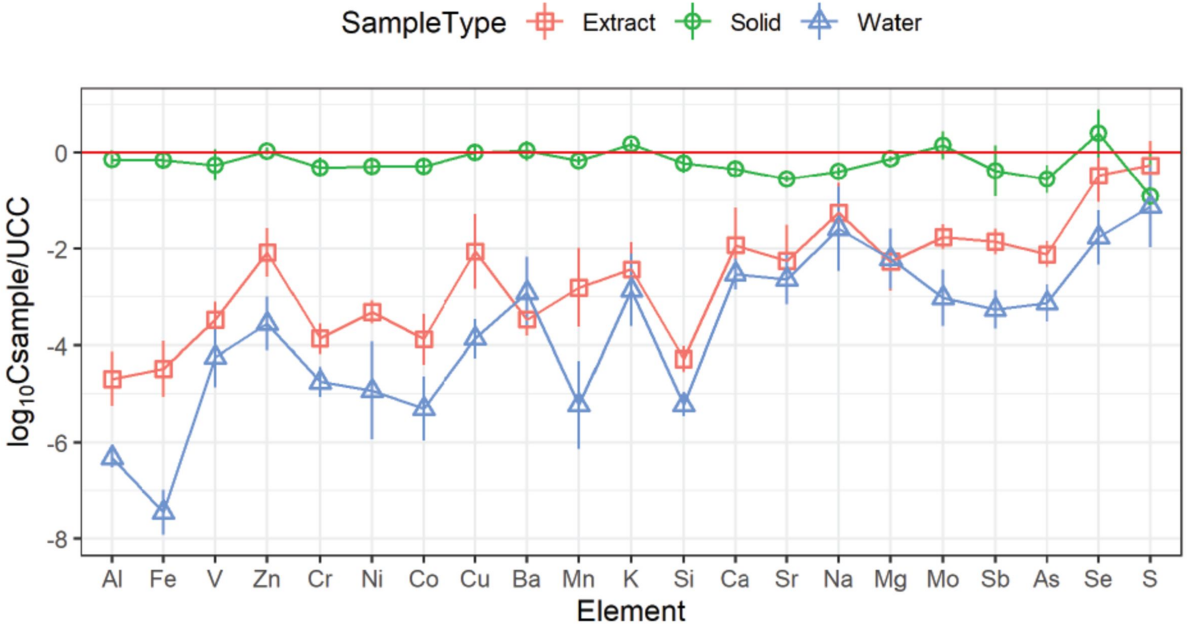
SampleType
Extract
Solid
Water
0
-2
-4
-6
-8
log10Csample/UCC
Al Fe V Zn Cr Ni Co Cu Ba Mn K Si Ca Sr Na Mg Mo Sb As Se S
Element

b)

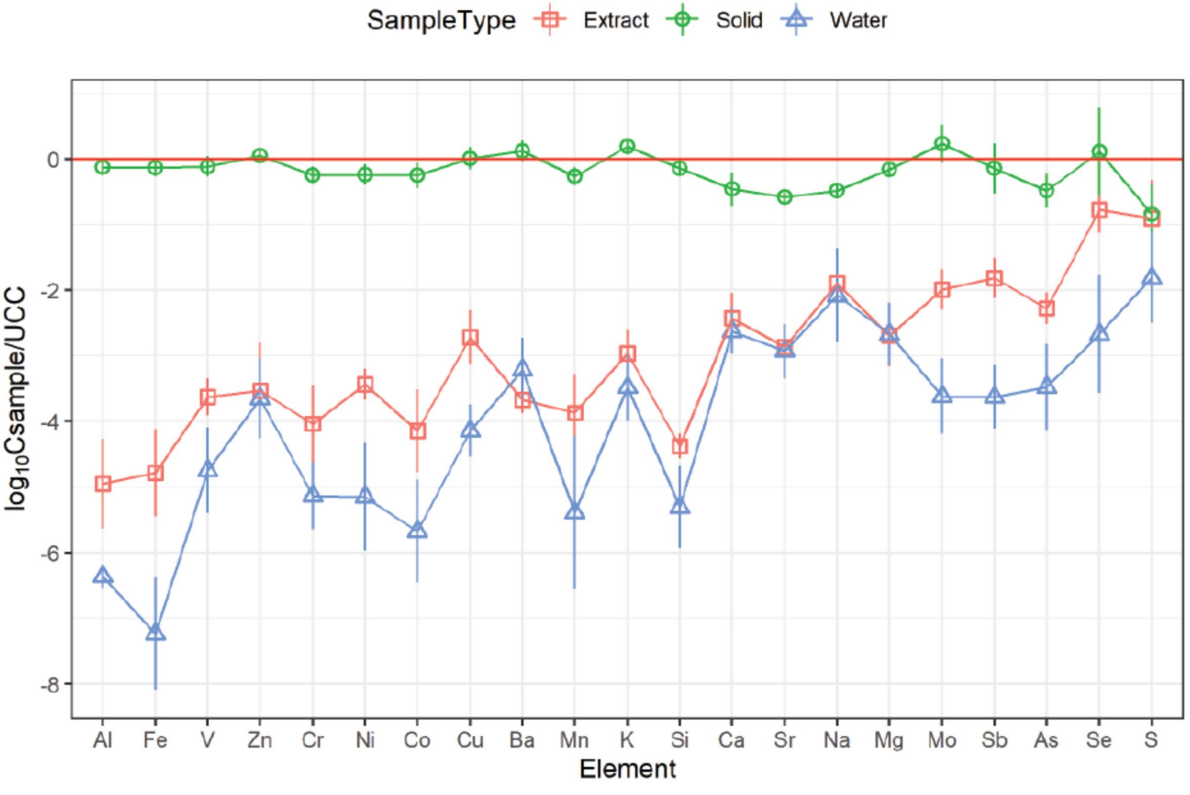
SampleType
Extract
Solid
Water
0
-2
-4
-6
-8
log10Csample/UCC
Al Fe V Zn Cr Ni Co Cu Ba Mn K Si Ca Sr Na Mg Mo Sb As Se S
Element

Figure 4.

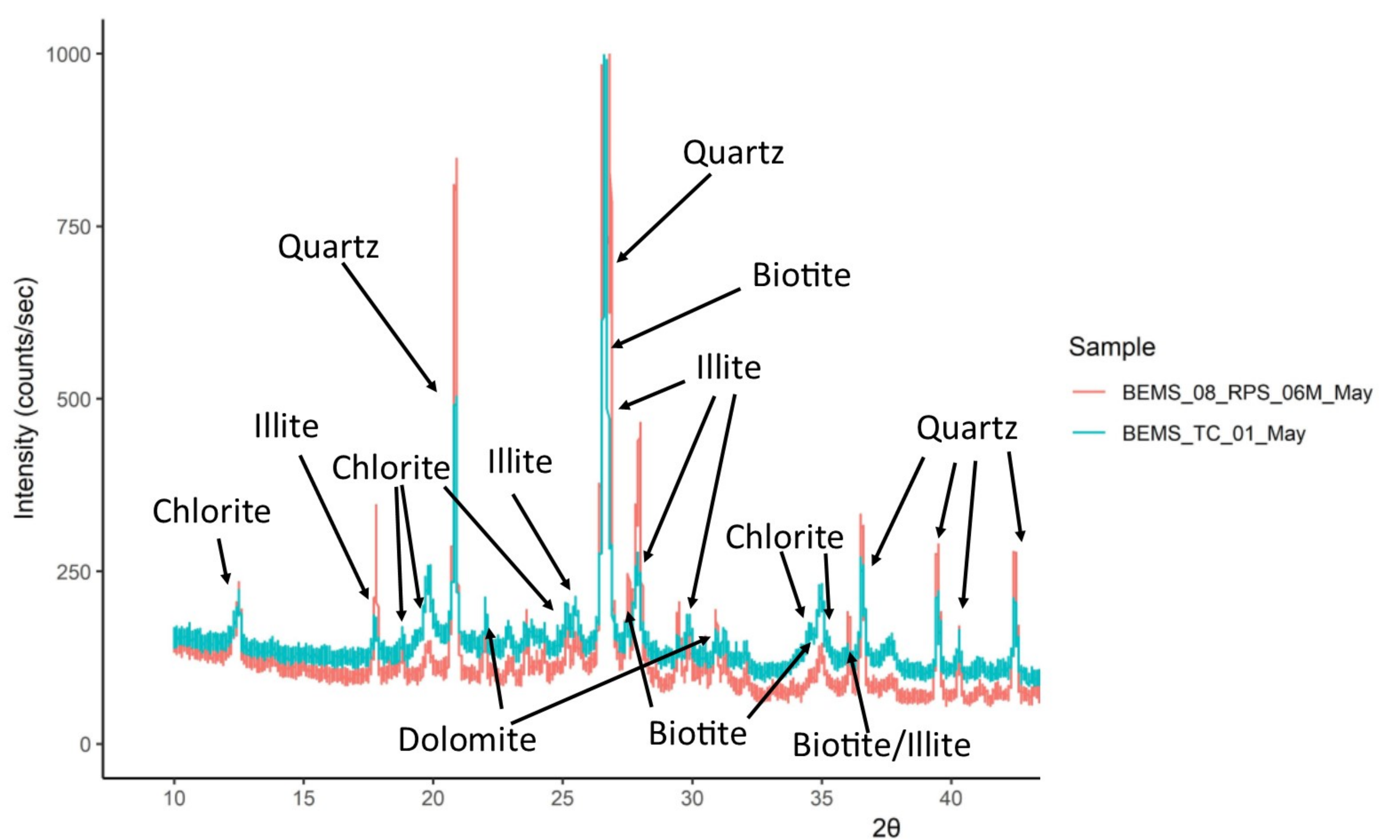
Intensity (counts/sec)
1000
750
500
250
0
10
15
20
25
30
35
40
2θ
Quartz
Quartz
Biotite
Illite
Illite
Chlorite
Illite
Chlorite
Quartz
Chlorite
Dolomite
Biotite
Biotite/Illite
Sample
BEMS_08_RPS_06M_May
BEMS_TC_01_May

Figure 5.

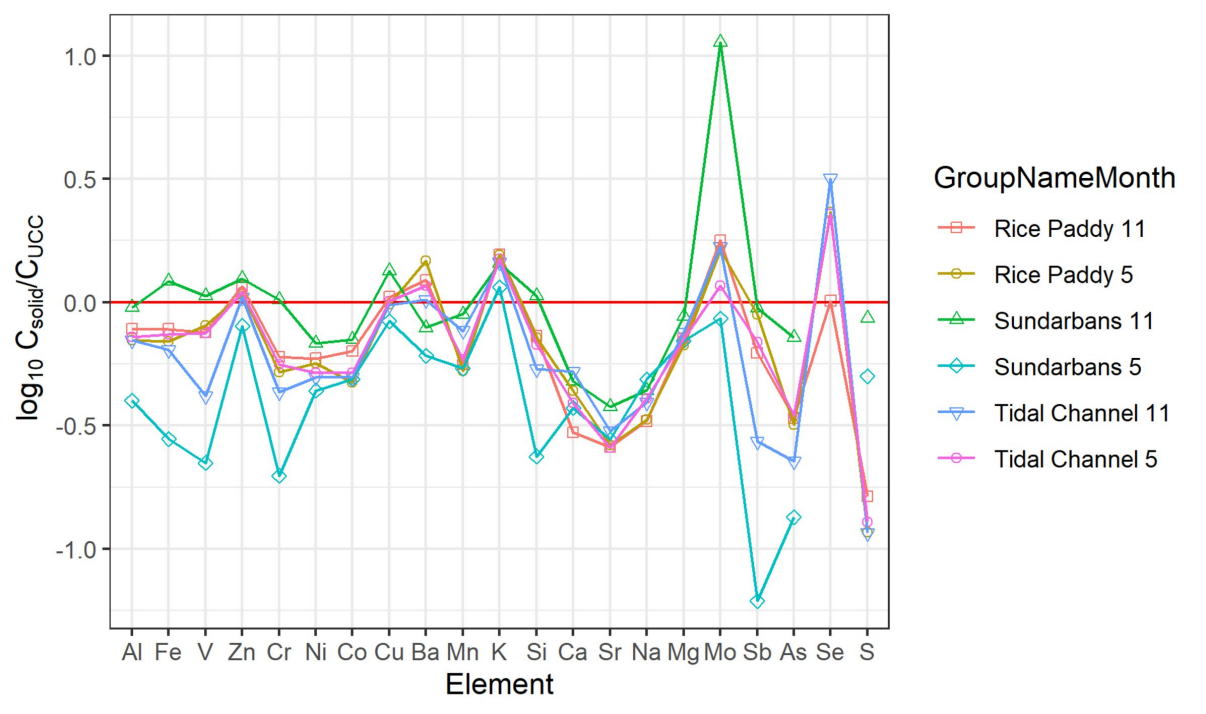
1.0
0.5
0.0
-0.5
-1.0
log10 Csolid/CUCC
Al Fe V Zn Cr Ni Co Cu Ba Mn K Si Ca Sr Na Mg Mo Sb As Se S
Element
GroupNameMonth
Rice Paddy 11
Rice Paddy 5
Sundarbans 11
Sundarbans 5
Tidal Channel 11
Tidal Channel 5

Figure 6.

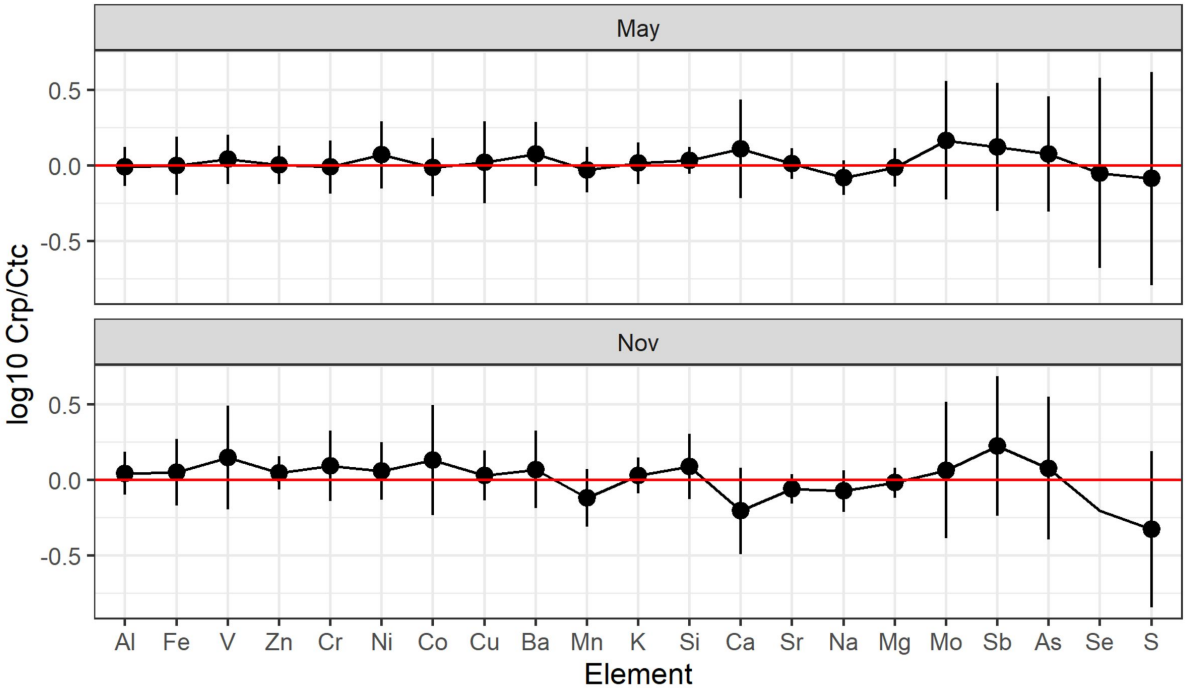
May
Nov
log10 Crp/Ctc
0.5
0.0
-0.5
Al
Fe
V
Zn
Cr
Ni
Co
Cu
Ba
Mn
K
Si
Ca
Sr
Na
Mg
Mo
Sb
As
Se
S
Element

Figure 7.

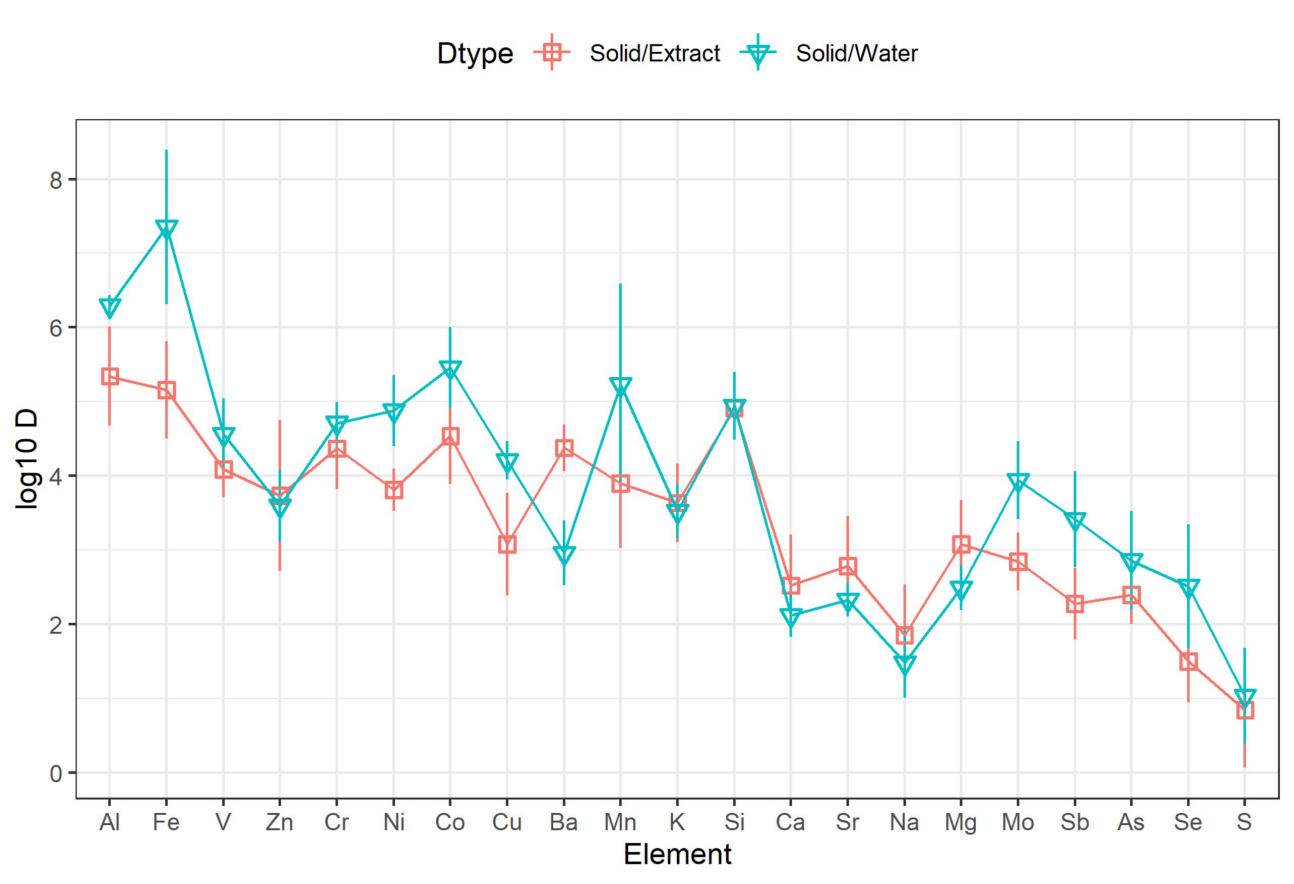
Dtype
Solid/Extract
Solid/Water
log10 D
8
6
4
2
0
Al
Fe
V
Zn
Cr
Ni
Co
Cu
Ba
Mn
K
Si
Ca
Sr
Na
Mg
Mo
Sb
As
Se
S
Element

Figure 8.

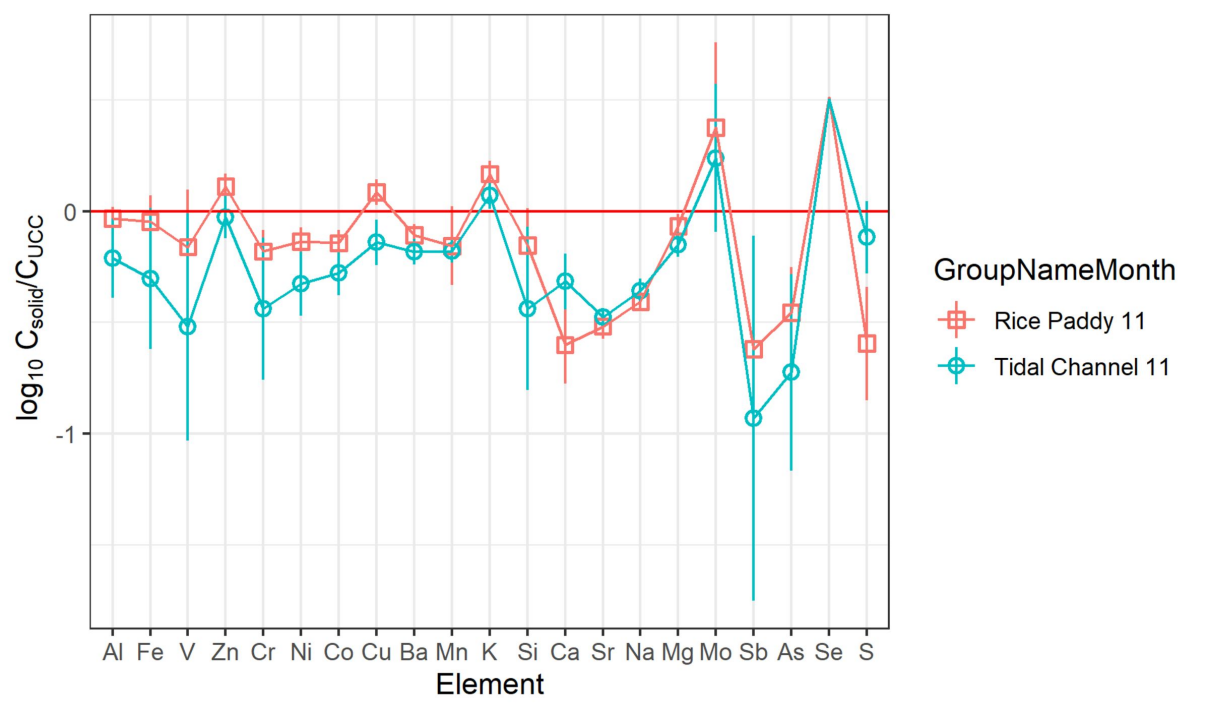
0
-1
log10 Csolid/CUCC
Al Fe V Zn Cr Ni Co Cu Ba Mn K Si Ca Sr Na Mg Mo Sb As Se S
Element
GroupNameMonth
Rice Paddy 11
Tidal Channel 11

Figure 9.

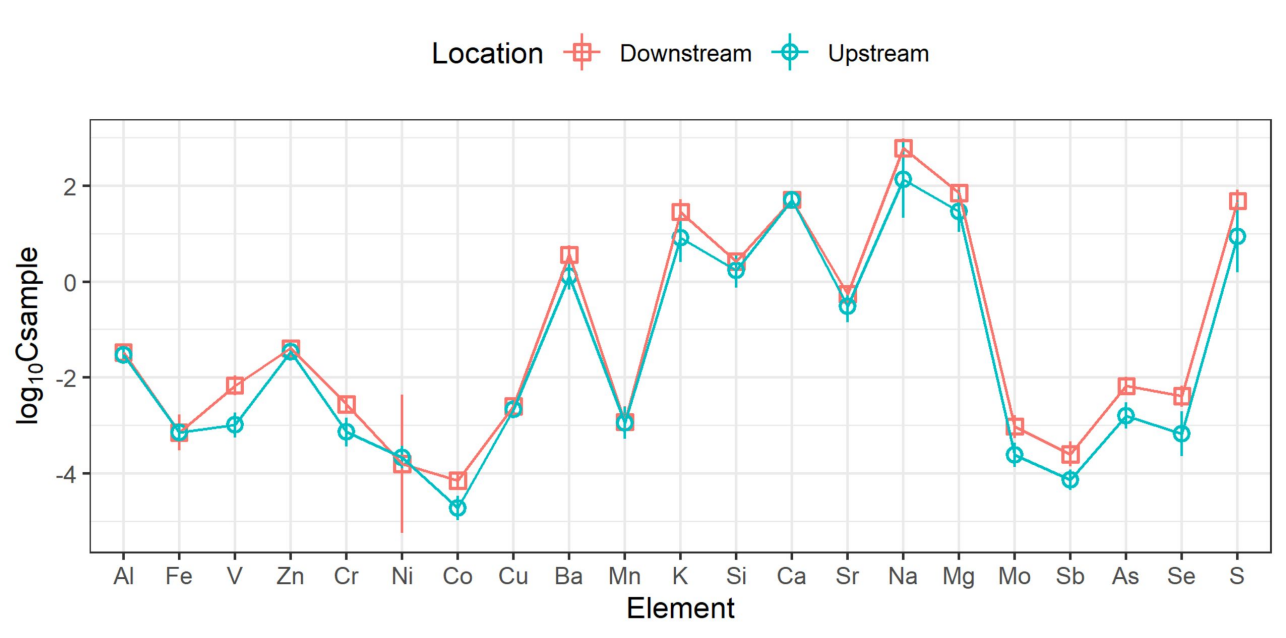
Location
Downstream
Upstream
log10Csample
2
0
-2
-4
Al
Fe
V
Zn
Cr
Ni
Co
Cu
Ba
Mn
K
Si
Ca
Sr
Na
Mg
Mo
Sb
As
Se
S
Element